REPORT DOCUMENTATION PAGE

Form Approved
OMB No. 0704-0188

1. REPORT DATE *(DD-MM-YYYY)*	**2. REPORT TYPE**	**3. DATES COVERED** *(From - To)*
January 2014	Journal Article	January 2014-April 2014

4. TITLE AND SUBTITLE

Thermal decomposition mechanisms of alkylimidazolium ionic liquids with CN-containing anions

5a. CONTRACT NUMBER
FA9300-06-C-0023

5b. GRANT NUMBER

5c. PROGRAM ELEMENT NUMBER

6. AUTHOR(S)

S.D. Chambreau, A.C. Schenk, A.J. Sheppard, G.R. Yandek, G.L. Vaghjiani, J. Maciejewski, C. J. Koh, A. Golan, S.R. Leone

5d. PROJECT NUMBER

5e. TASK NUMBER

5f. WORK UNIT NUMBER
Q0RA

7. PERFORMING ORGANIZATION NAME(S) AND ADDRESS(ES)

Air Force Research Laboratory (AFMC)
AFRL/RQRP
10 E. Saturn Blvd.
Edwards AFB, CA, 93524-7680

8. PERFORMING ORGANIZATION REPORT NO.

9. SPONSORING / MONITORING AGENCY NAME(S) AND ADDRESS(ES)

Air Force Research Laboratory (AFMC)
AFRL/RQR
5 Pollux Drive.
Edwards AFB, CA, 93524-7048

10. SPONSOR/MONITOR'S ACRONYM(S)

11. SPONSOR/MONITOR'S REPORT NUMBER(S)
AFRL-RQ-ED-JA-2014-037

12. DISTRIBUTION / AVAILABILITY STATEMENT
Approved for public release; distribution unlimited

13. SUPPLEMENTARY NOTES
Journal article published in the Journal of Physical Chemisty, Vol. #118, Issue #47, Nov 2014.
PA Case Number: #14111; Clearance Date: 13 Mar 14.

14. ABSTRACT

Due to the unusually high heats of vaporization of room-temperature ionic liquids (RTILs), volatilization of RTILs through thermal decomposition and vaporization of the decomposition products can be significant. Upon heating of these RTILs in vacuum, their gaseous products were detected experimentally via tunable vacuum ultraviolet photoionization mass spectrometry performed at the Chemical Dynamics Beamline 9.0.2 at the Advanced Light Source. Experimental evidence for di- and tri-alkylimidazolium cations and nitrile containing anions indicates thermal decomposition occurs through two pathways: deprotonation of the cation by the anion, and dealkylation of the imidazolium cation by the anion. Additional evidence supporting these mechanisms was obtained using thermal gravimetric analysis/mass spectrometry, gas chromatography/mass spectrometry and temperature-jump infrared spectroscopy. In order to predict the overall thermal stability in these ionic liquids, the ability to accurately calculate both the basicity of the anions and their nucleophilicity in the ionic liquid is critical. Both gas phase and condensed phase (polarizable continuum model) density functional theory calculations provide support for the decomposition mechanisms and a means to determine thermal stabilities for ionic liquids in general.

15. SUBJECT TERMS

16. SECURITY CLASSIFICATION OF:			**17. LIMITATION OF ABSTRACT**	**18. NUMBER OF PAGES**	**19a. NAME OF RESPONSIBLE PERSON**
					G. Vaghjiani
a. REPORT	**b. ABSTRACT**	**c. THIS PAGE**	SAR	41	**19b. TELEPHONE NO** *(include area code)*
Unclassified	**Unclassified**	**Unclassified**			661-275-5657

Standard Form 298 (Rev. 8-98)
Prescribed by ANSI Std. 239.18

Thermal decomposition mechanisms of alkylimidazolium ionic liquids with CN-containing anions

Steven D. Chambreau,[1] Adam C. Schenk,[2] Anna J. Sheppard,[2] Gregory R. Yandek,[2] Ghanshyam L. Vaghjiani[2,*]

John Maciejewski[3]

Christine J. Koh,[4] Amir Golan,[5] Stephen R. Leone[4,5]

1. ERC, Inc., Edwards Air Force Base, California, 93524, U.S.A.
2. Propellants Branch, Aerospace Systems Directorate, Air Force Research Laboratory, AFRL/RQRP, Edwards Air Force Base, California, 93524, U.S.A.
3. Department of Chemistry, University of Idaho, Moscow, ID, 83844, U.S.A.
4. Departments of Chemistry and Physics, University of California, Berkeley, California, 94720, U.S.A.
5. Lawrence Berkeley National Laboratory, Berkeley, California, 94720, U.S.A.

Abstract

Due to the unusually high heats of vaporization of room-temperature ionic liquids (RTILs), volatilization of RTILs through thermal decomposition and vaporization of the decomposition products can be significant. Upon heating of these RTILs in vacuum, their gaseous products were detected experimentally via tunable vacuum ultraviolet photoionization mass spectrometry performed at the Chemical Dynamics Beamline 9.0.2 at the Advanced Light Source. Experimental evidence for di- and tri-alkylimidazolium cations and nitrile containing anions indicates thermal decomposition occurs through two pathways: deprotonation of the cation by the anion, and dealkylation of the imidazolium cation by the anion. Additional evidence supporting these mechanisms was obtained using thermal gravimetric analysis/mass spectrometry, gas chromatography/mass spectrometry and temperature-jump infrared spectroscopy. In order to predict the overall thermal stability in these ionic liquids, the ability to accurately calculate both the basicity of the anions and their nucleophilicity in the ionic liquid is critical. Both gas phase and condensed phase (polarizable continuum model) density functional theory calculations provide support for the decomposition mechanisms and a means to determine thermal stabilities for ionic liquids in general.

Keywords: ionic liquids, thermal decomposition, synchrotron, VUV, photoionization efficiency, polarizable continuum model.

*Email: ghanshyam.vaghjiani@us.af.mil; Tel: 661-275-5657; Fax: 661-275-5471

INTRODUCTION

Ionic liquids (with m.p. ≤ 100 °C) consist of discrete ions and have distinctly different physical and chemical properties from molecular liquids. The most widely recognized characteristic of ionic liquids is their negligible vapor pressure, making them attractive candidates for replacements of volatile organic compounds commonly used as reaction solvents. In order to depress the melting point of ionic solids, it is necessary to reduce the Coulombic attraction between cations and anions. This can be achieved through functionalization of small, tightly-bound ions to create larger, more diffusely charged ions. Often, the reduction in Coulombic attraction between the ions results in glass formation rather than actual melting of the solid. In the successful synthesis of ionic liquids, their viscosities tend to remain unusually high, which can limit their usefulness as solvents.

The dicyanamide anion-based family of room-temperature ionic liquids (RTILs) exhibits some of the lowest viscosities of any known RTILs.[1] They can be easily prepared from the appropriate halide salts and silver dicyanamide and were the first RTILs to demonstrate hypergolic reactivity (spontaneous ignition) when mixed with white fuming nitric acid.[1,2] Ionic liquids are not only well known for their negligible vapor pressures but also for their thermal stability. Because of their extremely low affinity for protons, bis-trifluoromethylsulfonylamide (NTf_2^-) based RTILs can be thermally stable up to almost 700 K. While significant theoretical work has been done on RTILs in the gas phase and by force field methods and quantum mechanics/molecular mechanics (QM/MM),[3-7] predicting reaction energetics in the condensed phase is difficult due to the ionic nature of the solvent; the solvent effects on the relative stabilities of the reactants, transition states and products involved in the reaction will effect both the rate and free energy of reaction. The development and implementation of an accurate yet

efficient theoretical approach to investigate the condensed phase reaction energetics of ionic liquids is highly desirable. Recent work in this regard using the polarizable continuum model (PCM)[8] shows great promise in this application.

In this paper, we investigate the thermal stability of RTILs with CN containing anions such as dicyanamide using a combination of several experimental probes and theory. Thermal gravimetric analysis (TGA) yields the enthalpies of vaporization, and when coupled with electron-impact ionization mass spectrometry, the activation enthalpies for individual thermal decomposition pathways of the ionic liquid can be obtained. Identification of vaporized products is also confirmed using gas chromatography/mass spectrometry (GC/MS), thermal gravimetric analysis-Fourier transform infrared (TGA-FTIR) spectroscopy and temperature-jump (T-jump) FTIR techniques. Finally, tunable vacuum ultraviolet photoionization time of flight mass spectrometry (VUV-PI-TOFMS) is used to identify the masses and ionization potentials of the gas-phase species evolved above a heated RTIL in a vacuum. The trends in these results have led to predictive capabilities using density functional theory (DFT) and direct dynamics modeling (see accompanying paper) that should be applicable to predicting thermal stabilities of other RTILs.

EXPERIMENTAL

1-Butyl-3-methylimidazlium tricyanomethanide ($BMIM^+TCM^-$, >98% purity) and 1-butyl-3-methylimidazolium dicyanamide ($BMIM^+dca^-$, >99% purity) were purchased from Merck and used without further purification. 1-Ethyl-3-methylimidazolium dicyanamide ($EMIM^+dca^-$ ≥98.5% purity), 1-ethylimidazolium thiocyanate ($EMIM^+SCN^-$, ≥99% purity) and 1-butyl-3-methylimidazolium thiocyanate ($BMIM^+SCN^-$, ≥95% purity) were purchased from Fluka and used without further purification. 1-Butyl-3-methylimidazolium vinylogous

dicyanamide ($BMIM^+vdca^-$) was synthesized as described in reference [9]. 1-Ethyl-2,3-dimethylimidazolium dicyanamide ($EMMIM^+dca^-$) was synthesized according to the procedure in reference [1].

The T-jump experiment[10,11] was carried out on a rapid scan FTIR spectrometer with 4 cm^{-1} resolution and 10 msec time resolution between spectra. An ionic liquid sample of about 3 µL was analyzed after a 1F capacitor discharged approximately 17 volts across a nichrome ribbon, reaching maximum temperature in ~50 msec. The discharge of the capacitor triggered the FTIR spectrometer. The experiment was conducted with an initial temperature of 298 K and at 1 atmosphere pressure. Maximum temperatures recorded for the ILs are as follows: $BMIM^+SCN^-$ T_{max} = 461 K, $BMIM^+dca^-$ T_{max} = 684 K and $BMIM^+TCM^-$ T_{max} = 675 K.

The TGA and TGA-MS experiments were similar to those described previously.[12,13] Briefly, the non-isothermal TGA measurements were carried out with a temperature ramp rate of 10 K/min from 303-973 K, and the isothermal TGA measurements typically were carried out from 423-573 K in either 5 K or 10 K steps with a 30 minute hold time at each step.

Gas chromatography-mass spectrometry (GC-MS) analysis was run with the electron impact ionizer tuned to 15 eV. VUV-PI-TOFMS experiments included the improved effusive ionic liquid source[13] and the aerosol source[14] described previously.

THEORY

Hybrid density functional theory was applied at the M06/6-31+G(d,p) level of theory[15] to investigate these IL systems. M05 has been shown to provide a good level of theory for calculating energetics of ionic liquid systems (mean average deviation, MAD, of 9.5 kJ/mol),[16] and M06 is presumed to be as good if not better than M05 for our purposes. Stationary states of reactants, intermediates, transition states and products, as well as adiabatic photoionization

potentials were calculated using Gaussian09.[17] Transition states were confirmed to have a single imaginary frequency and through internal reaction coordinate analysis.

A variant of the quantum mechanical continuum solvation model SMD[18] known as the generic ionic liquid (SMD-GIL) model[19] was employed to calculate free energies in the ionic liquid condensed phase. The SMD-GIL solvent descriptor input parameters used for $EMIM^+dca^-$ as a solvent are e = 11.50, n = 1.4300, γ = 61.24, $\Sigma\alpha_2^H$ = 0.229, $\Sigma\beta_2^H$ = 0.265, φ = 0.2308, and ψ = 0.0000,[19] while φ = 0.2727 and 0.200 for $EMIM^+SCN^-$ and $EMIM^+TCM^-$, respectively. The fraction of non-hydrogen atoms that are electronegative halogen atoms (ψ) is zero for dca^-, SCN^-, TCM^- and $vdca^-$ containing ionic liquids and ψ = 0.0500 for $EMIM^+Br^-$. SMD-GIL calculations were carried out using M06/6-31+G(d,p) in Gaussian 09.[17]

RESULTS

The thermal decomposition of CN containing anionic RTILs was investigated using several complementary experimental probes, including thermal gravimetric analysis, thermal gravimetric analysis coupled to either a mass spectrometer or a Fourier transform infrared (FTIR) spectrometer, temperature-jump FTIR spectroscopy, GC/MS and tunable vacuum ultraviolet photoionization time of flight mass spectrometry. For brevity, a representative spectrum from each experimental technique will be presented here and the remainder of the data can be found in the supporting information. Numeric data is summarized in Tables 1-5.

Thermal Gravimetric Analysis

Thermal gravimetric analysis (TGA) is a measurement of the mass of a sample as it is heated, typically with an inert gas flowing over the sample. In an inert environment, the mass loss as the temperature increases can be the result of vaporization of the sample or of the thermal decomposition of the sample followed by subsequent vaporization of the thermal decomposition

products. For volatile species, simple evaporation takes place and 100% of the sample mass is lost due to vaporization of the intact species. The rate of evaporation is dependent on the enthalpy of vaporization of the species, the surface area of the sample, and the flow and molecular mass of inert gas over the sample.[20,21] For easily decomposing species, first decomposition must occur and the products must diffuse to the surface of the sample, where they can evaporate. Mass loss due to thermal decomposition processes can be less than 100% if thermal decomposition products have low volatility or form solids. The rate of thermal decomposition depends on the activation enthalpies for all decomposition pathways and is not dependent upon surface area of the sample.[20,21] The total mass loss rate by TGA is the sum of the mass loss from evaporation and the mass losses from all thermal decomposition processes which produce volatile species. However, because the evaporation and thermal decomposition rates are dependent on different factors, the enthalpy of vaporization for low-volatility species such as RTILs can be accurately determined by an isothermal analysis[22] and the thermal decomposition rates are better measured by fast heating rates. When the enthalpy of vaporization is comparable to or higher than the lowest activation enthalpy for thermal decomposition, then mass loss by thermal decomposition competes with or dominates over mass loss by evaporation.[12,23] Enthalpies of vaporization of RTILs range from 120 kJ/mol to over 200 kJ/mol, and thermal decomposition is a highly competitive process in these compounds.

The TGA of 1-ethyl-3-methylimidazolium dicyanamide, $EMIM^{+}dca^{-}$, indicates a mass loss onset (non-zero slope) temperature above 510 K with two distinct peaks at 590 and 690 K (Figure 1a). Fitting the lowest temperature peak in an Arrhenius plot (Figure 1b) yields an enthalpy for the overall mass loss rate of 151.7 ± 14.5 kJ/mol (± 95% confidence limits) at an average temperature (T_{avg}) of 566 K (Table 1). In order to determine the enthalpy of

vaporization (ΔH_{vap}) of $EMIM^+dca^-$, isothermal TGA analysis (described previously)[13,22] yields a ΔH_{vap} value of ΔH_{vap} = 128.3 ± 19.2 kJ/mol (T_{avg} = 473 K), which when corrected to 298 K using $\Delta_g^l C_p$ of -72.0 J/K (see Table 1 and discussion for details),[5] gives $\Delta H_{vap}(298)$ = 140.9 ± 19.2 kJ/mol.

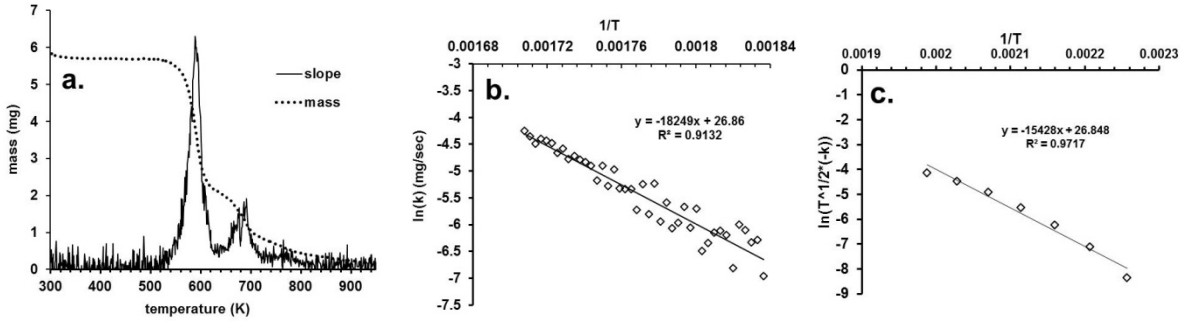

Figure 1. Thermal gravimetric analysis of 1-ethyl-3-methylimidazolium dicyanamide: a) TGA, b) Arrhenius plot of slope from Figure 1a, c) isothermal TGA to determine ΔH_{vap} = 140.9 ± 19.2 kJ/mol (298 K).

Table 1. Experimental enthalpies of activation, $\Delta H^{\ddagger}$(overall), and vaporization, ΔH_{vap} (at T_{avg} and 298 K) determined by TGA. Enthalpies are in kJ/mol, $\Delta_l^g C_{pm}^o$ is in J/mol•K and temperatures are in K.

Ionic liquid	$\Delta H^{\ddagger}$(overall)	T_{avg}	ΔH_{vap}	T_{avg}	$\Delta_l^g C_{pm}^o$	ΔH_{vap}(298)
$EMIM^+dca^-$	151.7 ± 14.5	566	128.3 ± 19.2	473	-72.0[a] ± 3.3	140.9 ± 19.2
$BMIM^+dca^-$	159.5 ± 10.2	560	133.1 ± 5.0	488	-72.5[a] ± 3.3	146.9 ± 5.0
$EMMIM^+dca^-$	268.4 ± 50.9	618	185.2 ± 14.2	513	-70[*]	200.3 ± 14.2
$EMIM^+SCN^-$	118.0 ± 3.7	535	150.7 ± 10.8	458	-60.8[b] ± 2.8	160.4 ± 10.8
$BMIM^+SCN^-$	165.7 ± 5.0	517	168.6 ± 9.2	448	-70.6[b] ± 3.2	179.9 ± 9.2
$BMIM^+TCM^-$[13]	183.0 ± 4.3	582	126.0 ± 6.2	473	-78.9[c] ± 3.6	139.8 ± 6.2
$BMIM^+vdca^-$	105.1 ± 25.3	475	62.1 ± 25.3	453	-70[*]	73.0 ± 25.3

[a]reference [24], [b]reference [25], [c]references [26,27], [*]estimated value- see text for details.

For $EMIM^+dca^-$ and several other CN containing anionic RTILs, there are several peaks in the TGA and the mass loss does not reach 100% at high temperature. This indicates that there are several different thermal decomposition processes occurring in different temperature

regimes, and that some solid is formed which is not volatile. Previous work on dicyanamide-based ionic liquids indicates that the dicyanamide anion can polymerize when heated,[28] perhaps through a melamine intermediate.[29,30] This will be discussed in more detail in the discussion section.

Thermal Gravimetric Analysis-Mass Spectrometry

A powerful enhancement to standard TGA is to couple the TGA to a mass spectrometer via a heated capillary tube. Volatile species evolved from the TGA can then be identified by their mass-to-charge ratios (m/z) and their fragmentation patterns. Furthermore, by monitoring a product species parent mass as a function of temperature, the activation enthalpy for its formation can be calculated using an Arrhenius-type analysis. The major species detected by TGA-mass spectrometric analysis of $EMIM^+dca^-$ are m/z = 82 and 96 (Figure 2a) and an Arrhenius plot for these masses (Figure 2b) yields the activation enthalpies for their formation, $\Delta H^{\ddagger}_{96}$ = 160 ± 16 kJ/mol and $\Delta H^{\ddagger}_{82}$ = 175 ± 17 kJ/mol at T_{avg} = 505 K. A conservative estimate of ± 10% was assigned to the uncertainties in $\Delta H^{\ddagger}$ due to possible systematic errors arising from mass transport (related to the chemical's vapor pressure) differences between the TGA and the mass spectrometer and ion transmission efficiency differences in the mass spectrometer itself. $\Delta H^{\ddagger}$ values calculated for selected masses of all ionic liquids are seen in Table 2.

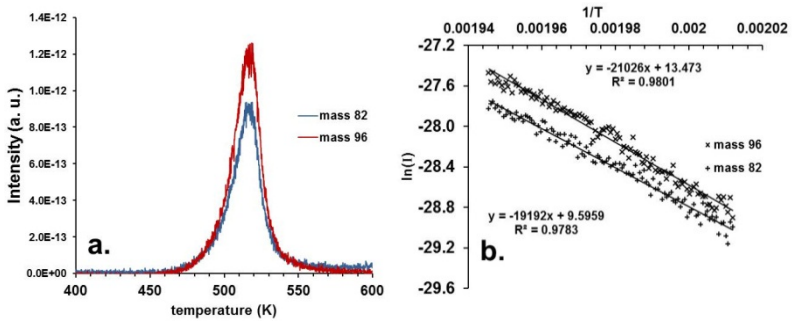

Figure 2. a) TGA-MS analysis of $EMIM^+dca^-$: mass 82 (methylimidazole) and 96 (ethylimidazole), and b) Arrhenius plot of data from Figure 2a: $\Delta H^{\ddagger}_{96}$ = 159.6 ± 2.3 kJ/mol (505 K), $\Delta H^{\ddagger}_{82}$ = 174.8 ± 2.4 kJ/mol (505 K).

Table 2. Experimental enthalpies of activation, $\Delta H^{\ddagger}$, for individual masses (at T_{avg}) determined by TGA-MS analysis. Enthalpies are in kJ/mol, m/z values are in amu and temperatures are in K. Uncertainties are estimated to be ± 10%.

Ionic liquid	$\Delta H^{\ddagger}$	m/z	$\Delta H^{\ddagger}$	m/z	T_{avg}
$EMIM^+dca^-$	160 ± 16	96	175 ± 17	82	505
$BMIM^+dca^-$	150 ± 15	82	162 ± 16	97	510
$EMMIM^+dca^-$	140 ± 14	96	137 ± 14	110	530
$BMIM^+TCM^-$	128 ± 13	78	98 ± 10	82	525
$EMIM^+SCN^-$	128 ± 13	73	109 ± 11	82	478
	126 ± 13	87	110 ± 11	96	478

Vacuum Ultraviolet Photoionization Time of Flight Mass Spectrometry

Representative vacuum ultraviolet time-of-flight mass spectrometry (VUV-TOFMS) data for $EMIM^+dca^-$ can be seen in Figure 3. Figure 3a shows a contour plot of the photoion intensities with a VUV photon energy range of 7.4-10.0 eV at an effusive source temperature of T=473 K, and Figure 3b is the corresponding photoionization mass spectrum at 9.0 eV. Photoionization efficiency (PIE) curves for masses 82, 96, 110 and 150 are seen in Figure 3c-d, and the total ion intensities (sum over all photon energies) of these masses are plotted as a function of effusive source temperature in Figure 3e. Photoion appearance energies were determined for the major photoions by fitting the PIE curves to the function $\alpha(E-E_o)^2$ near the photoionization threshold, as described previously,[4,14,31] and are reported along with their calculated (M06/6-31+G(d,p), 298 K) adiabatic ionization energies and relative ion abundances in Table 3.

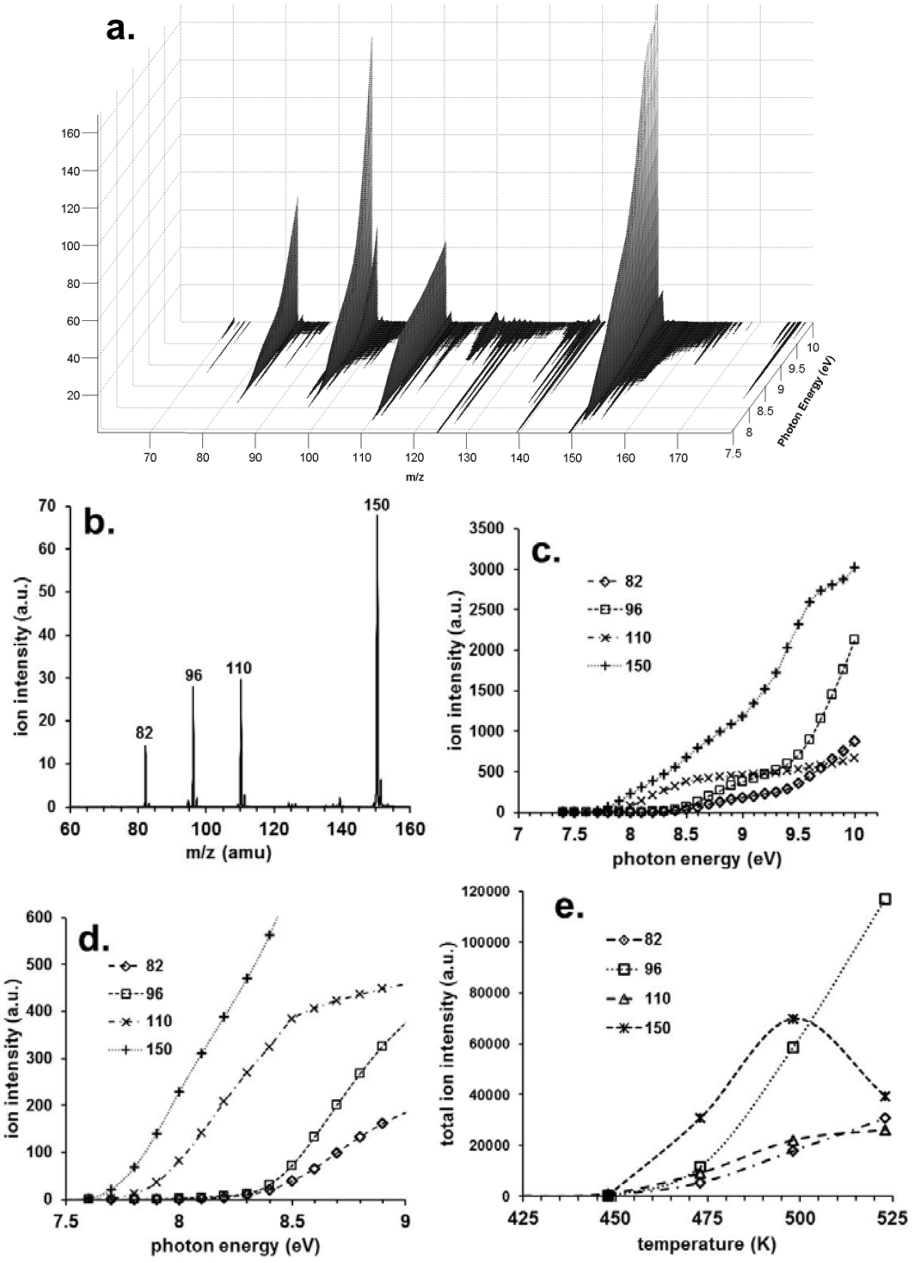

Figure 3. a) VUV-PI-TOFMS analysis of $EMIM^{+}dca^{-}$ at 473 K from 7.4 to 10.0 eV photon energy, and b) 9.0 eV photon energy, c) PIE curves for masses in (b), d) expanded view of the photoion thresholds from (c), and e), total ion count/relative abundance of the photoions from 450 to 525 K.

Table 3. VUV-TOFMS data for all ionic liquids investigated. ΔG_{298} values are in eV.

EMIM$^+$dca$^-$, 463 K			
mass (amu)	**appearance energy (eV)**	**ΔG_{298} M06/6-31+G(d,p)**	**relative abundance (%)**
27	13.4 ± 0.2	13.3 ± 0.2	4.4
82	8.3 ± 0.2	8.4 ± 0.2	14.2
96	8.3 ± 0.2	8.3 ± 0.2	23.9
110	7.6 ± 0.2	7.7 ± 0.2	11.4
150	7.5 ± 0.2	7.6 ± 0.2	45.3
BMIM$^+$dca$^-$, 483 K			
mass (amu)	**appearance energy (eV)**	**ΔG_{298} M06/6-31+G(d,p)**	**relative abundance (%)**
27	13.4 ± 0.2	13.3 ± 0.2	4.0
82	8.4 ± 0.2	8.4 ± 0.2	20.5
97	7.6 ± 0.2	ND	18.0
124	8.2 ± 0.2	8.3 ± 0.2	15.6
137	7.9 ± 0.2	ND	15.1
178	7.6 ± 0.2	8.3 ± 0.2	5.4
EMMIM$^+$dca$^-$, 423 K			
mass (amu)	**appearance energy (eV)**	**ΔG_{298} M06/6-31+G(d,p)**	**relative abundance (%)**
96	7.7 ± 0.2	8.0 ± 0.2	17.0
110	7.9 ± 0.2	7.9 ± 0.2	6.1
124	6.0 ± 0.5	6.1 ± 0.2	52.8
125	7.2 ± 0.5	7.2 ± 0.2	23.9
EMIM$^+$SCN$^-$, 467 K			
mass (amu)	**appearance energy (eV)**	**ΔG_{298} M06/6-31+G(d,p)**	**relative abundance (%)**
27	13.3 ± 0.2	13.3 ± 0.2	3.4
73	8.2 ± 0.2	9.1 ± 0.2 (CH_3NCS)	23.2
82	8.4 ± 0.2	8.4 ± 0.2	8.8
87	9.1 ± 0.2	9.0 ± 0.2 (CH_3CH_2NCS)	4.6
96	8.3 ± 0.2	8.3 ± 0.2	30.9
142	7.1 ± 0.3	7.2 ± 0.2	29.1
BMIM$^+$SCN$^-$, 493 K			
mass (amu)	**appearance energy (eV)**	**ΔG_{298} M06/6-31+G(d,p)**	**relative abundance (%)**
27	13.4 ± 0.2	13.3 ± 0.2	4.4
73	9.1 ± 0.2	9.1 ± 0.2 (CH_3NCS)	29.3
82	8.3 ± 0.2	8.4 ± 0.2	19.7
97	9.3 ± 0.2	ND	9.3
124	8.1 ± 0.2	8.3 ± 0.2	15.1
137	9.2 ± 0.2	ND	20.3
170	8.8 ± 0.2	7.1 ± 0.2	1.8
BMIM$^+$TCM$^-$, 433 K			
mass (amu)	**appearance energy (eV)**	**ΔG_{298} M06/6-31+G(d,p)**	**relative abundance (%)**
82	8.2 ± 0.2	8.4 ± 0.2	1.1
96	7.6 ± 0.2	ND	67.9
110	7.7 ± 0.2	ND	2.0
124	8.2 ± 0.2	8.3 ± 0.2	4.6
137	7.6 ± 0.2	ND	17.8
139	7.1 ± 0.3	6.9 ± 0.2	3.4
229	6.6 ± 0.5	7.3 ± 0.2	3.1
BMIM$^+$vdca$^-$, 413 K			
mass (amu)	**appearance energy (eV)**	**ΔG_{298} M06/6-31+G(d,p)**	**relative abundance (%)**
96	7.7 ± 0.2	ND	1.2
110	8.0 ± 0.2	ND	8.0
124	8.2 ± 0.2	8.3 ± 0.2	2.1
137	7.6 ± 0.2	ND	8.0
178	7.1 ± 0.3	8.3 ± 0.2	43.6

VUV-PI-TOFMS for 1-butyl-3-methylimidazolium dicyanamide ($BMIM^+dca^-$) was extensively performed for this species. Figures 4a-c represent two VUV-TOFMS spectra which are generated by low temperature evaporation of $BMIM^+dca^-$ aerosols as described previously[14] (Figures 4a and b, 380 K), or by the effusive ionic liquid source at 483 K and photoionized at 10.0 eV (Figure 4c). Figure 4d is from gas chromatograph-mass spectrometric (GC/MS) analysis of $BMIM^+dca^-$ with a 15 eV electron-impact ionization source, indicating a parent ion mass of m/z = 178. In Figure 5, the scaled mass spectra indicate the changes in the $BMIM^+$ cation signal as a function of temperature in the range of 438-483 K photoionized at 12.0 eV and averaged over 5 million repeller pulses.

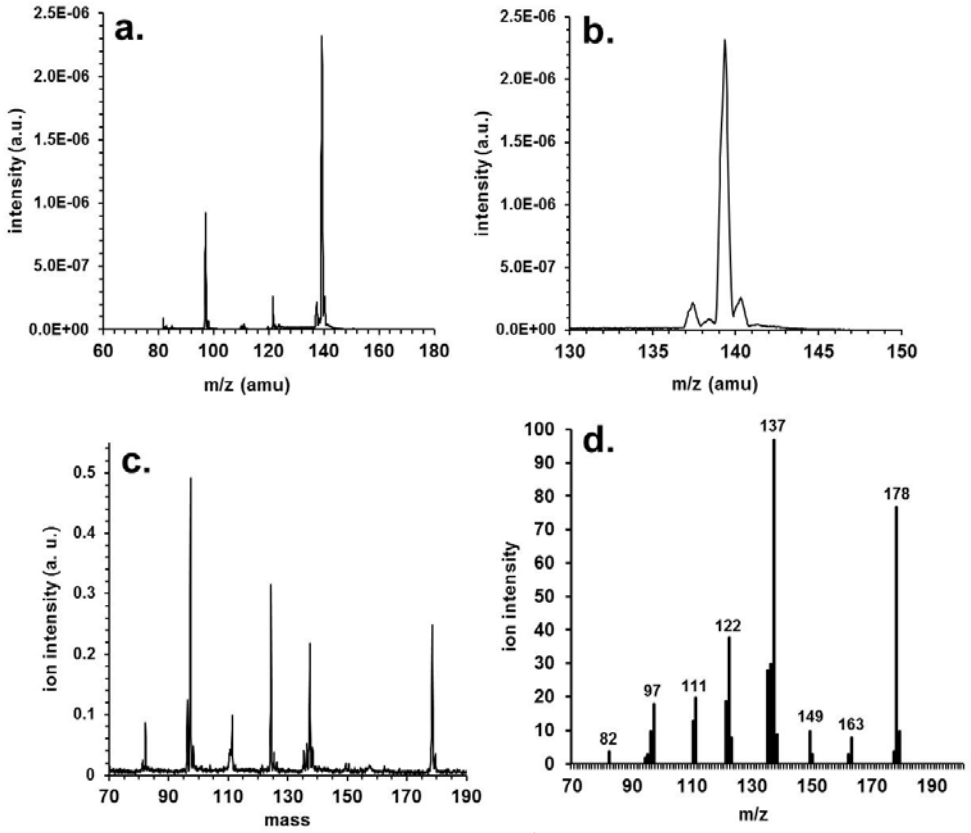

Figure 4. a) VUV-PI-TOFMS spectrum of $BMIM^+dca^-$ aerosol at 380 K and 10.0 eV and b) expanded view of the $BMIM^+$ cation at m/z 139 from (a), c) $BMIM^+dca^-$ spectrum from the effusive source at 483 K and 10.0 eV and d) GC/MS analysis of $BMIM^+dca^-$ with 15 eV electron impact ionization energy.

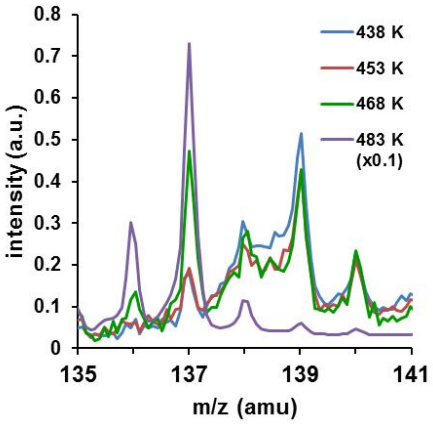

Figure 5. VUV-PI-TOFMS spectrum of $BMIM^+dca^-$ for the effusive source in the range of 438-483 K at 12.0 eV photoionization energy, 5 million shots, traces scaled for comparison.

Temperature-jump Fourier Transform Infrared Spectroscopy

Likely due to polymerization, no coproducts containing the dca^- or TCM^- anions were observed using the TGA-MS or the effusive source in the VUV experiments. Therefore, temperature-jump Fourier transform infrared spectroscopy (T-jump FTIR) was employed in an attempt to rapidly vaporize the products before they could polymerize. The experimental design is based on previous work by Brill and coworkers.[10,11] T-jump FTIR spectroscopy results for $BMIM^+SCN^-$, $BMIM^+TCM^-$ and $BMIM^+dca^-$ are seen in Figure 6.

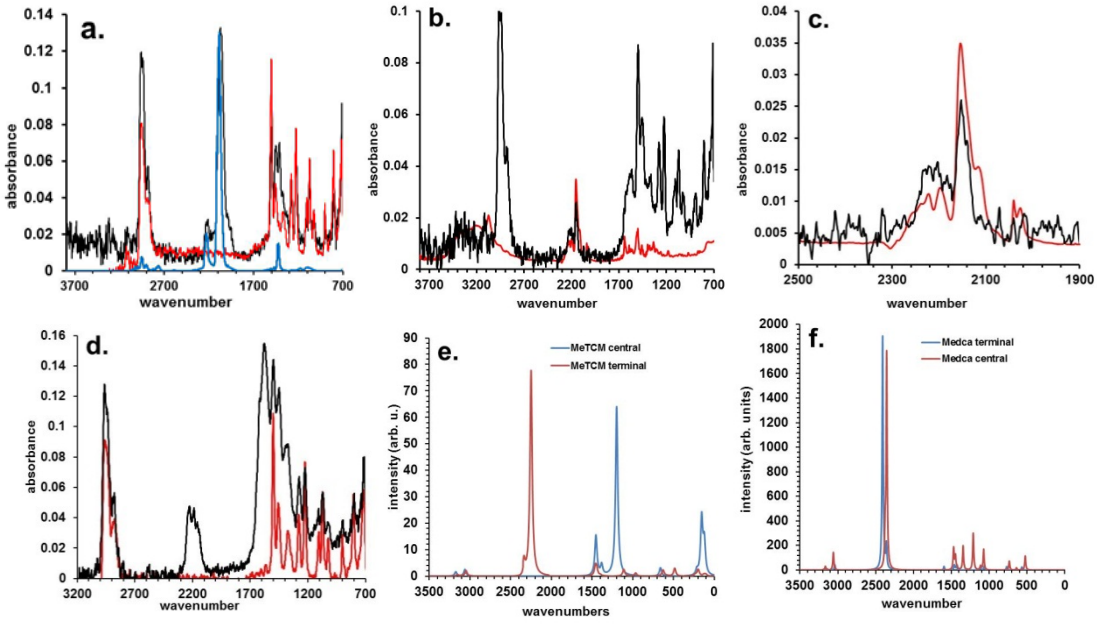

Figure 6. T-jump FTIR spectra of a) $BMIM^+SCN^-$ decomposition products (black) compared to a H_3CNCS (blue, ref [32]) and 3:1 ratio of butylimidazole and methylimidazole (red), b) $BMIM^+TCM^-$ decomposition products (black) and linear ketenimine (red, from reference [33]), c) an expanded view of the central peak in (b), d) $BMIM^+dca^-$ decomposition products (black) and butylimidazole (red), e) DFT IR simulation of methylated TCM^-, and f) DFT IR simulation of methylated dca^-.

DISCUSSION

Thermal Gravimetric Analysis

In comparing the TGA data for all of the investigated CN-containing anionic ionic liquids, the only IL to achieve near 100% mass loss are the thiocyanates 1-ethyl-3-methylimidazilium thiocyanate, $EMIM^+SCN^-$, and 1-butyl-3-methylimidazolium thiocyanate, $BMIM^+SCN^-$. All of the other ILs investigated have mass losses <100%, indicating solid residue formation, likely through polymerization of the anions or their thermal decomposition products.[28,29] This indicates that the thermal decomposition products in the SCN^- systems either do not easily polymerize or are able to vaporize before polymerization can occur. From Table 1, based on the overall $\Delta H^{\ddagger}$ values, the trend in stability, from least to most stable, is: $BMIM^+vdca^-$

< $EMIM^+SCN^-$ < $EMIM^+dca^-$ < $BMIM^+dca^-$ < $BMIM^+SCN^-$ < $BMIM^+TCM^-$ < $EMMIM^+dca^-$. Similarly, from Table 1, based on the overall ΔH_{vap} values, the trend in enthalpies of vaporization, from lowest to highest, is: $BMIM^+vdca^-$ < $BMIM^+TCM^-$ < $EMIM^+dca^-$ < $BMIM^+dca^-$ < $EMIM^+SCN^-$ < $BMIM^+SCN^-$ < $EMMIM^+dca^-$, which is consistent with previous experimental and theoretical heats of vaporization for these ILs.[5,34-37] The heat of vaporization determined for $BMIM^+vdca^-$ is unusually low (Table 1), and is likely attributable to mass loss from thermal decomposition instead of from vaporization of the intact IL. If this is true, then based on enthalpies of vaporization, the most volatile IL is $BMIM^+TCM^-$. This species has been detected directly in the vapor phase and has one of the highest vapor pressures of known ILs.[13,38] Clearly, for the thiocyanate ILs, since their overall activation enthalpies determined by TGA are significantly lower than their enthalpies of vaporization, thermal decomposition is strongly favored over vaporization at moderate temperatures (T<573 K) in these ILs. Conversely, for the tricyanomethanide and trialkylimidizolium dicyanamide ILs, their enthalpies of vaporization are significantly lower than their overall thermal decomposition activation enthalpies, and vaporization is favored over thermal decomposition at moderate temperatures (T<573 K), as has been observed previously for dialkylimidazolium carboxylate ionic liquids.[39] For the dialkylimidazolium dicyanamides, where their overall thermal decomposition activation enthalpies and enthalpies of vaporization are fairly similar, it is likely that thermal decomposition and vaporization are competing below T = 573 K. It is important to note that, according to Trouton's Rule (ΔS_{vap} ~ 10.5R), entropic contributions are typically larger for vaporization than for thermal decomposition processes in the condensed phase discussed here (ΔS < 4R), and this effectively lowers the free energy of vaporization more than for thermal decomposition versus considering only the enthalpies in these two competing processes.

In order to accurately determine the enthalpy of vaporization of ionic liquids under standard conditions (298 K), it is important to accurately determine $\Delta_l^g C_{pm}^o$, the change in molar heat capacity from liquid to the gas phase.[36,37,40-43] A recent study by Verevkin[5] and coworkers have demonstrated that $\Delta_l^g C_{pm}^o$ can be estimated by:

$$\Delta_l^g C_{pm}^o = -2R - (C_{pm}^o - C_{vm}^o)_l \quad (1)$$

where:

$$(C_{pm}^o - C_{vm}^o)_l = \frac{\alpha_p^2}{K_T} V_m T \quad (2)$$

and α_p is the thermal expansion coefficient, K_T is the isothermal compressibility, and V_m is the molar volume of the ionic liquid. Prior to this work, $\Delta_l^g C_{pm}^o$ values were simply estimated to be 100 J/mol•K and this assumption was the main source of error in measuring standard enthalpies of vaporization of ionic liquids. For this work, literature values for α_p and K_T for five of the ionic liquids were used to calculate the $\Delta_l^g C_{pm}^o$ values in Table 1. The 100 J/mol•K value for $\Delta_l^g C_{pm}^o$ used previously was based on much work with the bis-trifluorosulfonylamide anion-based ionic liquids, which have large molar heat capacities (500-1000 J/mol•K at 298 K[5]). The ionic liquids investigated here have smaller molar heat capacities (~300 J/mol•K) and would be expected to have smaller $\Delta_l^g C_{pm}^o$ values as well. In fact, the $\Delta_l^g C_{pm}^o$ values in Table 1 average about 70 J/mol•K, and this value was used as an estimate for $\Delta_l^g C_{pm}^o$ for $EMMIM^+dca^-$ and for $BMIM^+vdca^-$, where no α_p or K_T values were available. This more accurate value for $\Delta_l^g C_{pm}^o$ decreases the standard enthalpies of vaporization for these ionic liquids by an average of 5.1 kJ/mol relative to those using the $\Delta_l^g C_{pm}^o$ = -100 J/mol•K value.

Thermal Gravimetric Analysis-Mass Spectrometry

Since the TGA results do not discriminate between vaporization and the thermal decomposition pathways available, TGA-MS is better suited for analyzing specific reaction pathways by monitoring volatile thermal decomposition products as a function of temperature; vaporization of ILs is not likely to be detected, as the ILs will condense in the capillary coupling the TGA to the mass spectrometer. Major mass peaks that were detected are listed in Table 2 along with their activation enthalpies of formation, which were calculated using an Arrhenius type analysis on the low temperature regime of the TGA-MS plots in Figure 2a and in the supplementary information.

TGA-MS results for the thermally unstable $BMIM^+vdca^-$ were complex and difficult to interpret, likely due to multiple decomposition pathways, and will not be discussed here. The next most sensitive IL to thermal decomposition, $EMIM^+SCN^-$, evolves masses at m/z 73, 82, 87 and 96 with activation enthalpies of (T_{avg} = 478 K) $\Delta H^{\ddagger}_{73}$ = 128 ± 13 kJ/mol, $\Delta H^{\ddagger}_{82}$ = 109 ± 11 kJ/mol, $\Delta H^{\ddagger}_{87}$ = 126 ± 13 kJ/mol and $\Delta H^{\ddagger}_{96}$ = 110 ± 11 kJ/mol (uncertainty estimated at 10%), respectively, and a small signal at m/z 142 which was too small to determine the thermal decomposition activation enthalpy. M/z 27 was difficult to detect due to interference from the large m/z 28 N_2 carrier gas signal. Note that these activation enthalpies are quite close to the overall thermal decomposition activation enthalpy determined by TGA of $\Delta H^{\ddagger}$ = 114.9 ± 3.6 kJ/mol. It is likely that these products are CH_3NCS (73), methylimidazole (82), CH_3CH_2NCS (87) and ethylimidazole (96) formed through an S_N2 type reaction whereby the SCN^- anion attacks the alkyl groups on the imidazolium cation. Mass 142 will be discussed in the next section.

For $BMIM^+dca^-$ and $EMIM^+dca^-$, the major product masses detected were 82 and 97, and 82 and 96, respectively. While the 82 and 96 masses are likely methyl- and ethylimidazole

formed via an S_N2 reaction similar to the thiocyanate ILs, the structure of mass 97 isn't clear. A very small signal at m/z 124 was detected for $BMIM^+dca^-$ that corresponds to the formation of butylimidazole, but the signal was too small to determine a thermal decomposition activation enthalpy for this species. The relatively small signal for butylimidazole is perhaps due to the lower vapor pressure of butylimidazole versus methyl- and ethylimidazole. For $EMMIM^+dca^-$, the primary masses detected were 110 and 96, corresponding to the S_N2 formation of 1-ethyl-2-methylimidazole and 1,2-dimethylimidazole.

Finally, for $BMIM^+TCM^-$, masses were detected via TGA-MS at 78, 82, 96, 107 and 124. While masses at m/z 82 and 124 are likely methylimidazole and butylimidazole, the source of m/z 78, 96 and 107 aren't clear, and further investigation is warranted.

Vacuum Ultraviolet Photoionization-Time of Flight Mass Spectrometry

It is accepted that for many aprotic ionic liquids they evaporate as intact ion pairs: C^+A^- (*l*) → C^+A^- (*g*) and that upon ionization of these gaseous ion pairs, dissociation to the cation C^+ and the radical A is facile: $C^+A^- \rightarrow C^+A + e^- \rightarrow C^+ + A + e^-$.[3,4,44] Due to the very high detection sensitivity afforded at the Chemical Dynamics Beamline at the Advanced Light Source, the mass signals resulting from the ion pairs and those from thermal decomposition products or even trace contaminants or previous IL experiments needed to be carefully differentiated. In many cases, the thermal decomposition products are detected at lower source temperatures than, or simultaneously with, the ionic liquid vapors.

A common feature amongst the dialkylimidazolium ionic liquids investigated in this work was the significant loss of 1 amu from the $EMIM^+$ cations, loss of 2 amu from the $BMIM^+$ cations, and loss of 1 amu from the $EMMIM^+$ cation to a lesser extent. A second trend throughout these ILs was the appearance of a mass peak in between the mass of the cation and

the ion pair, namely the mass of the ion pair – 27 amu. Finally, as was mentioned previously, there is strong evidence of S_N2 dealkylation of the imidazolium by the anions. Previous work on ILs with more basic anions has determined that neutralization can occur through proton transfer from C2 on the imidazolium to the anion, leading to the formation of a neutral carbene[45,46] and an acid (protonated anion) which can then vaporize and be detected, unless the protonated anion can undergo polymerization to form a solid. In the case of $EMIM^+dca^-$, the carbene is detected at m/z 110 with a photoionization energy of 7.6 ± 0.2 eV (Figure 3c) and matches well with the M06 calculated ionization energy for the EMIM carbene (EMIM**:**) of 7.7 ± 0.2 eV. While m/z 110 was not detected in the case of $EMIM^+SCN^-$, the formation of m/z 142 and HCN strongly suggest that these products are formed via the EMIM: carbene intermediate (Figure 7). The extent of carbene formation should be dependent on two factors: the basicity of the anion and the stability of the carbene itself. Table 4 illustrates the relative strength of the base by determining the free energy of acidity: essentially how much free energy it takes to separate a proton from the acid HA. The higher the value of ΔG_{acid}, the more stable the acid HA and the less likely the anion will remain as a negative anion in the presence of acidic hydrogens. Species with ΔG_{acid}(g) values smaller than 300 kcal/mol (1255 kJ/mol) are considered to be superacids[47] and these tend to make good candidates as anions for IL synthesis. The generic ionic liquid (SMD-GIL) variant[19] of the polarizable continuum model was employed here to calculate the ΔG_{acid}(l) values in an imidazolium ionic liquid and with water as a solvent as well (Table 4). The solvent effect on these systems reduces the free energy ΔG_{acid} values from around 1200 kJ/mol to around 520 kJ/mol in both the ionic liquid and in water. This reduction in energy is primarily driven by the large solvation energy of a proton (~550 kJ/mol) versus anions (~210 kJ/mol on average) in the condensed phases (table in SI). Based on the ΔG_{acid} values in Table 4, the expected trend for

formation of C^+-1 amu photoions to appear in the VUV mass spectrum would be: SCN^- > dca^- > $vdca^-$ > TCM^-. With the exception of $EMIM^+SCN^-$ which has a short-lived m/z 110 as described below, this trend is confirmed in the VUV experiments, and, in fact, no C^+-1 amu peak was detected for $BMIM^+TCM^-$. The ΔG_{acid} values for H^+ loss from the C2 of $EMIM^+$ and $BMIM^+$ or from the C2 methyl of $EMMIM^+$ are 262.9, 264.6 and 261.8 kJ/mol, respectively, and essentially are the same within the margin of error of M06 and therefore the anion basicity is independent of cation for these cations. Note that the deprotonation of $EMMIM^+$ leads to formation of a stable methylene product at m/z 124 and not a reactive carbene species.

The nitrate and bromide anions were included in this analysis to compare their relative basicities with the nitrile containing anions. Previous gas phase acidity calculations indicated that the dca^- anion was less basic than the NO_3^- anion, and the equilibrium HNO_3 + dca^- ↔ NO_3^- + Hdca would favor protonation of the NO_3^-.[2] From these SMD-GIL calculations, the solvation effect stabilizes Hdca more than HNO_3 and NO_3^- more than dca^-, and would result in a spontaneous proton transfer from HNO_3 to dca^-. This solvation effect might help to explain the high reactivity of dicyanamide-based ionic liquids towards nitric acid.[2]

Table 4. Calculated free energies of acidity, ΔG_{acid}, in the gas phase and in the condensed phase by SMD-GIL and SMD (water) at the M06/6-31+G(d,p) level of theory.

	ΔG_{acid} (g)		ΔG_{acid} (l)		ΔG_{acid} (l)
acid	**(kJ/mol)**		**SMD-GIL (kJ/mol)**		**SMD-H_2O (kJ/mol)**
HNCS	1332.5	HNCS	607.0	HNCS	549.5
HNO_3	1306.7	HNCNCN	578.0	HNCNCN	521.8
HSCN	1274.2	HNO_3	566.6	Hvdca 04	515.2
HNCNCN	1272.6	Hvdca 01	565.2	Hvdca 01	514.6
NCNHCN	1234.6	Hvdca 04	564.9	NCNHCN	495.9
Hvdca 01	1212.1	NCNHCN	550.3	HNO_3	494.9
Hvdca 04	1203.3	HSCN	548.8	HSCN	492.6
HTCM (central)	1197.1	HTCM (central)	537.9	HTCM (central)	490.5
HTCM (terminal)	1188.7	HTCM (terminal)	533.9	HTCM (terminal)	483.9
Hvdca 02	1152.7	Hvdca 03	518.1	Hvdca 03	471.4
Hvdca 03	1146.1	Hvdca 02	517.6	Hvdca 02	468.6

Hvdca 01 = terminal NH, Hvdca 02 = $-CCN_1H$, Hvdca 03 = $-CCN_2H$, Hvdca 04 = central NH

It is well known that carbenes are highly reactive species,[45,46,48-50] and it is likely that these carbenes formed upon heating of the ILs are also involved in the formation of the species detected at m/z C^+A^- - 27 amu seen in the dca^- and SCN^- systems. Additional evidence for these species was seen in the TGA-MS of $EMIM^+SCN^-$ (SI) and in the GC/MS trace of $BMIM^+dca^-$ (Figure 4d), indicating that these products are thermodynamically stable. By determining the experimental VUV ionization potential (IP) of the m/z 27 photoion to be = 13.4 ± 0.2 eV, this mass can be identified as HCN (I.P. = 13.4 eV[51]). Detailed *ab initio* analyses of the possible mechanisms of formation of m/z 142 + HCN form $EMIM^+SCN^-$ are shown in Figure 7. The proposed mechanism first involves the proton transfer to the SCN^- anion to form HNCS, which is more basic than HSCN (Table 4). This is followed by the rapid nucleophilic attack of the carbene at the carbon in HNCS. The S can then migrate to C2 on the imidazole ring, followed by HNC elimination from C2, which rapidly converts to HCN. This process effectively replaces the C2 proton in the ion pair with a sulfur atom, resulting in a neutral thioimidazole, which could explain the lack of m/z 110 for $EMIM^+SCN^-$ in the VUV-TOFMS spectra if the reaction is sufficiently fast once the carbene is formed. This scheme has been generalized to CN-containing anions in Figure 8. The more basic the anion is, and to a lesser extent, the more electrophilic the protonated anion is, the more likely this reaction is going to occur. These species are detected at temperatures slightly higher than the detection temperature of the carbenes, which is consistent with the small activation barrier involved in the nucleophilic attack of the carbene on the protonated anion (step 2 to 3 in Figure 7). This type of mechanism may also explain the addition of an oxygen atom to the EMIM cation in the thermal decomposition of $EMIM^+NO_3^-$.[52] Although sulfur addition to C2 on the dialkylimidazolium cation through an n-heterocyclic carbene (NHC) intermediate has been demonstrated previously,[46] to our knowledge, this is the

first report of the NCN-ylidene being formed. This route could possibly be useful for a one-pot synthesis for these NCN imidazolium-ylidene species without the need for flammable solvents.

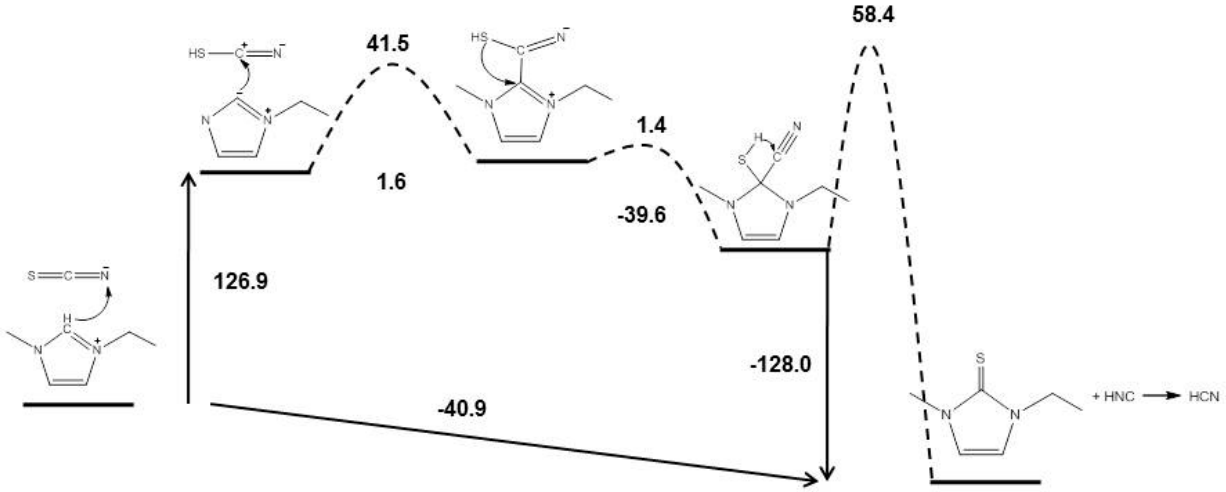

Figure 7. M06/6-31+G(d,p) free energy reaction profile of the thermal decomposition of $EMIM^{+}SCN^{-}$ leading to the formation of m/z 142 and HCN. Values are in kJ/mol

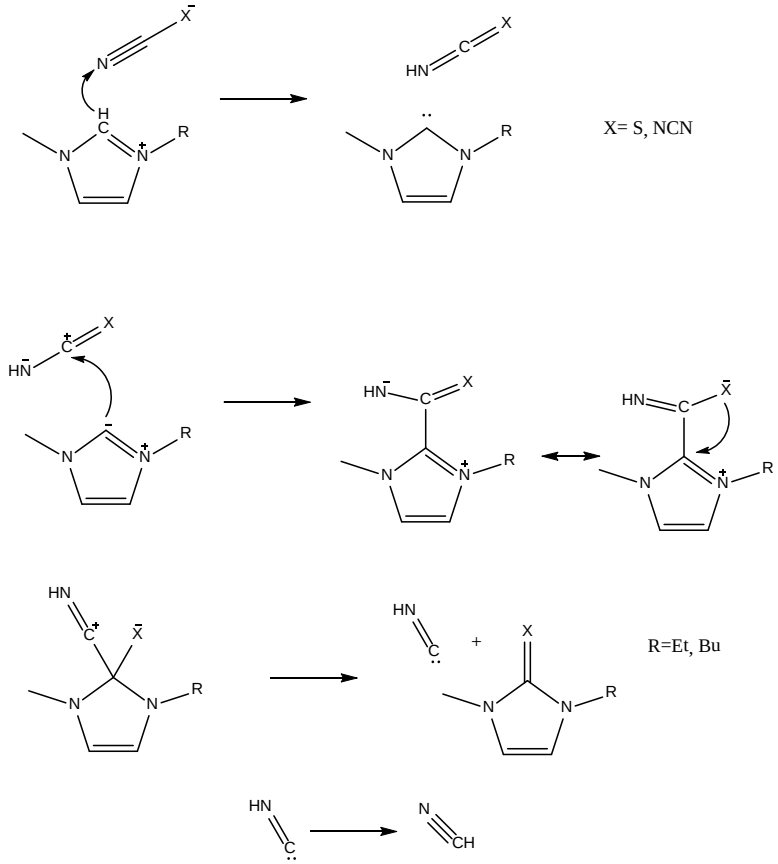

Figure 8. Generalized scheme for the addition-elimination reaction through a carbene intermediate.

At even higher temperatures, the third major decomposition pathway indicated in the VUV-PI-TOFMS experiments is the S_N2 alkyl abstraction by the anion, as has been proposed previously in the 1-ethyl-3-methylimidazolium bromide[12] and 1-ethyl-3-methylimidazolium nitrate[52] ionic liquids. Due to steric constraints, the abstraction of the methyl group on the imidazolium cation is expected to be more facile than the bulkier ethyl or butyl groups, and this is evidenced by the lower activation energies for the formation of ethylimidazole or butylimidazole versus methylimidazole (Table 2 and supported by DFT calculations). Further evidence that this S_N2 reaction occurs is the detection of CH_3NCS and CH_3CH_2NCS in the thermal decomposition of $EMIM^+SCN^-$: The experimental I.P.s of mass 73 and 87 are 8.2 ± 0.2 eV and 9.1 ± 0.2 eV, respectively, while the M06 I.P. values are 9.1 ± 0.2 eV and 9.0 ± 0.2 eV for R-NCS (R=CH_3, CH_3CH_2-) and 9.9 ± 0.2 eV and 9.7 ± 0.2 eV for R-SCN (R=CH_3, CH_3CH_2-), giving a better match with the RNCS species. The temperature-jump experiments described below support this conclusion as well.

The appearance of the m/z 137 peak in the $BMIM^+$ ILs indicates that the $BMIM^+$ cation loses 2 hydrogens quite easily. It is possible that the mechanism for this involves the formation of the BMIM**:** carbene species which could rapidly react to lose a second hydrogen. In Figure 5, the progression from the intact $BMIM^+$ cation (m/z 139, formed from dissociative photoionization of the vaporized ion pair) through the carbene (m/z 138) to m/z 137 as the temperature is raised from 438 to 483 K can be seen. At 438 and 453 K, the predominant peak is at m/z 139, with smaller peaks at m/z 138 and 137. At 468 K, the m/z 139 and 137 peaks are nearly equal in intensity, but the ratio of the m/z 139/138 peaks does not change significantly.

This seems to indicate that if the m/z 137 species is formed via the BMIM**:** carbene (m/z 138), the carbene reacts quickly to form m/z 137 and is not detected. At 483 K, the m/z 139 peak nearly disappears and m/z 137 dominates, indicating that the rate of conversion of m/z 139 to 137 has surpassed evaporation, and the intensities of m/z 138 and 139 are consistent with ^{13}C isotopes resulting from the m/z 137 species. An interesting possibility is that the length of the butyl group allows the end of the butyl group to access the C2 carbene structure via rotations around the N-C and C-C bonds in the butyl group (see Scheme 1), whereas in the EMIM**:**, the ethyl group is too short to react with the C2 carbene and does not lose a second hydrogen:

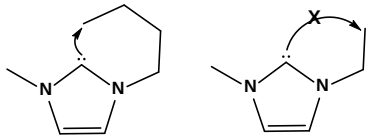

Scheme 1.

Bicyclic ionic liquids have been prepared from the BMIM cation-based ionic liquids,[53] which means that cyclization of the butyl group should be kinetically accessible to the BMIM carbene cation. It could be possible that m/z 137 is the result of conversion of the $BMIM^+$ cation to the bicyclic cation species (B^+, m/z 137) in the condensed phase through the carbene intermediate, which can then evaporate as a B^+A^- ion pair that undergoes dissociative photoionization to produce m/z 137 and A**·**. If the resulting B^+A^- has a lower enthalpy of vaporization than $BMIM^+A^-$ then the m/z 137 peak would dominate the mass spectrum versus m/z 139. Another possibility for the formation of m/z 137 is as an ionization fragment of m/z 178 (see GC/MS spectrum, Figure 4d). However, additional research is needed to understand and explain this phenomenon.

Temperature-jump Fourier Transform Infrared Spectroscopy

Additional evidence for the S_N2 alkyl abstractions is seen in the T-jump experiment involving $BMIM^+SCN^-$, which in Figure 6a clearly shows the formation of CH_3NCS. For $BMIM^+SCN^-$, the intense peak at 2080 cm^{-1} and smaller peak at ~2200 cm^{-1} in Figure 6a suggests the formation of $SCN\text{-}CH_3$,[32] whereas $NCS\text{-}CH_3$ would have only a single peak at 2180 cm^{-1},[54] which is consistent with the VUV-PI-TOFMS results for $BMIM^+SCN^-$. No HNCS or HSCN was detected. These experiments also indicate the demethylation of the imidazolium cation to form butylimidazole and a methylated anionic species for $BMIM^+TCM^-$ and $BMIM^+dca^-$ ILs. The methylated dicyanamide (with two –CN groups) and methylated tricyanomethanide (three –CN groups) products likely polymerize when heated slowly, which would explain their absence in the VUV-TOFMS experiments, while methylated thiocyanate (with only one –CN group) cannot polymerize. For $BMIM^+TCM^-$, Figures 6b and 6c demonstrate a good match from 2100 to 2300 cm^{-1} with data from Finnerty et. al.[33] (used with permission), indicating methylation of the terminal nitrogen on the tricyanomethanide species, $CH_3\text{-}NCC(CN)_2$ rather than at the central carbon, $CH_3\text{-}C(CN)_3$. This is consistent with the M06 IR simulation in Figure 6e indicating that there should be no peaks in this region for the centrally methylated species. For $BMIM^+dca^-$ (Figure 6d), there are two peaks which arise from the methylated product at ~1600 cm^{-1} and ~2200 cm^{-1}. From the M06 IR simulation (Figure 6f), both the terminally and centrally methylated dicyanamide species show peaks in the 2200 cm^{-1} range, so the indentity of this product isn't clear. However, the simulated spectrum of the terminally methylated species shows a small peak at ~1600 cm^{-1} whereas the centrally methylated dicyanamide simulation does not show any peaks in this region. Also, previous DFT calculations indicate that the barrier to form the terminally methylated dicyanamide should be lower than for the centrally methylated product.[55]

Density Functional Theory Modeling

In order to verify the thermal decomposition mechanisms proposed based on the experimental evidence, hybrid density functional theory was applied at the M06/6-31+G(d,p) level of theory to these IL systems. M05 has been shown to provide a good level of theory for calculating energetics of ionic liquid systems (mean average deviation, MAD, of 9.5 kJ/mol),[16] and M06 is presumed to be as good if not better than M05 for our purposes. Stationary states of reactants, intermediates, transition states and products, as well as adiabatic photoionization potentials were calculated. A representative free energy profile for $EMIM^+SCN^-$ is shown in Figure 7.

Adiabatic ionization potentials (I.P.) calculated for the proposed species match well with the experimentally determined photoionization energies (Table 3). For EMIM**:** (m/z 110), the experimentally determined value is 7.6 ± 0.2 eV and the M06 value is 7.7 ± 0.2 eV. Similarly, for the addition-elimination reactions (S: m/z 142 and 170, -NCN: 150 and 178 for $EMIM^+$ and $BMIM^+$, respectively, Figure 8), all of the experimental I.P.s match the M06 calculated I.P.s within 0.2 eV. In some cases, these species are detected at energies below the threshold to detect C^+ from dissociative ionization of the ion pair, which is an indication that these species are formed in the condensed phase and are not a result of dissociative photoionization.

Polarizable Continuum Model: SMD-GIL Method

In order to accurately represent the energetics involved in the liquid phase reactions of ionic liquids, a comparison was made between the gas phase $\Delta G_{acid}(g)$ calculations (Table 4) and the M06 energetics in Figure 7a and the corresponding energetics using the recent adaptation of the continuum solvation model (SMD) referred to as the generic ionic liquid (SMD-GIL) model.[19] This model parameterizes the PCM to accurately determine free energies of solvation

and benchmarks to known experimental values, resulting in mean unsigned error (MUE) in free energy values of less than 1.85 kcal/mol. For $EMIM^+dca^-$, the SMD-GIL solvent model has a MUE of 0.65 kcal/mol. For determining the ΔG_{acid}(l) in the condensed phase, the estimated error in these calculations is $\pm\sqrt{3}(0.65)$ kcal/mol, or ±1.1 kcal/mol (±4.7 kJ/mol). The results for ΔG_{acid} are seen in Table 4.

The results of the SMD-GIL calculations for $EMIM^+SCN^-$ are seen in Figure 9. It is interesting to note that, relative to the gas phase, the free energy of solvation using the PCM model stabilizes the ion pair much more than the other neutral/molecular species and transition states. Intuitively, this makes sense, as the ionic solvent will more readily solvate ions versus molecular species. The effect of lowering the free energy of the IL ion pair reactant more than the free energies of the intermediates, transition states and products increases the initial free energy of activation in the condensed phase relative to the gas phase. Interestingly, the gas phase prediction of the activation barrier for the S_N2 reactions for $EMIM^+SCN^-$ incorrectly predicts the methyl abstraction to have a higher barrier than the ethyl abstraction, but the PCM model correctly predicts the methyl abstraction to be the more facile route.

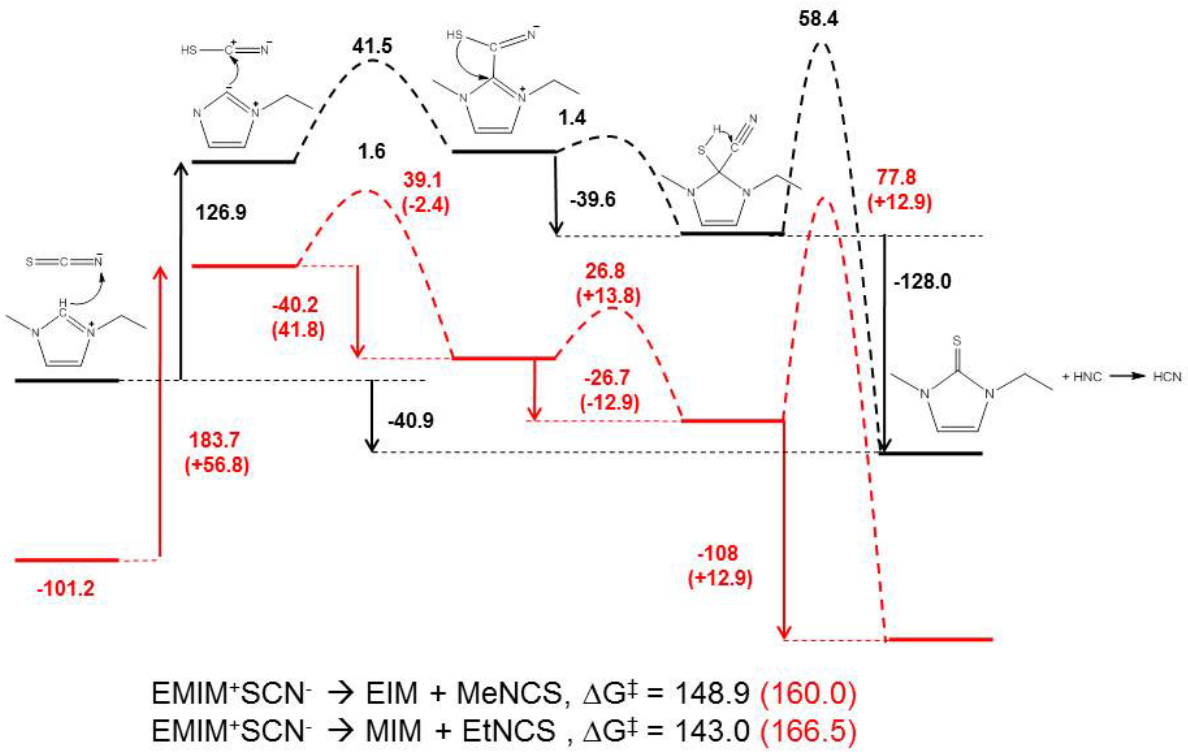

Figure 9. Free energy reaction profile comparison of gas phase (black) and SMD-GIL (red) using M06/6-31+G(d,p) for the formation of m/z 142 from $EMIM^+SCN^-$. Values are in kJ/mol.

Nucleophilicity of Anions

While nucleophilicity scales[56] are well defined for many species in common solvents in which synthetic reactions are carried out (i.e., in H_2O, hexane, etc.), the relative nucleophilicity of the nitrile containing anions towards alkyl abstraction from the dialkylimidazolium cations is not readily apparent. In order to evaluate the nucleophilicity of these CN containing anions, transition states of the S_N2 type methyl abstractions-the major alkyl abstraction reaction from the dialkylimidazolium cations (Scheme 2)- were located in both the gas phase and in the condensed phase using SMD-GIL to determine their free energies of activation (Table 5). The pathways with the lowest activation free energies would be expected to have the fastest alkyl abstraction rates and therefore be the most nucleophilic. The free energies of activation for S_N2 methyl

abstraction for SCN^-, dca^-, TCM^- and Br^- (for comparison to our previous study)[12] to form CH_3NCS $CH_3N{=}C{=}NCN$, $CH_3N{=}C{=}C(CN)_2$ and CH_3Br, respectively, are seen in Table 5.

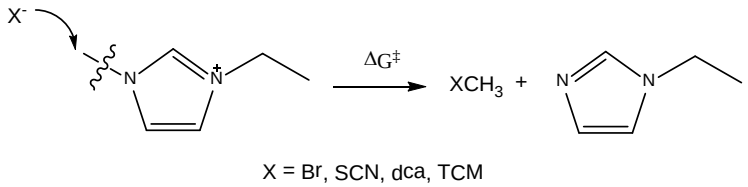

Scheme 2.

Table 5. Free energies of activation for S_N2 methyl abstraction from $EMIM^+$ by the anion calculated at the M06/6-31+G(d,p) level of theory and using the generic ionic liquid (GIL) model to simulate the condensed phase methyl abstraction.

IL	**ΔG*** (gas: M06) (kJ/mol)	**ΔG*** (liquid: GIL) (kJ/mol)	**ΔΔG** (gas→liquid) (kJ/mol)
$EMIM^+Br^-$	138.6	134.6	-4.0
$EMIM^+dca^-$	163.6	158.2	-5.4
$EMIM^+SCN^-$	148.9	160.0	11.1
$EMIM^+TCM^-$	175.8	181.5	5.7

From Table 5, the trend of relative nucleophilicities of the anions is, in decreasing nucleophilic strength: $Br^- > SCN^- > dca^- > TCM^-$. It is interesting to note that difference in the free energy of activation does not change significantly (from -4.0 to 11.1 kJ/mol) upon going from the M06 gas phase calculation to the GIL condensed phase calculation, which contrasts with the large shift in the free energy of activation for the initial proton transfer in the SCN^- system (Figure 9). Also, the trend for anion basicity and relative nucleophilicity are the same, but it is not apparent if this is coincidental or if this is a general trend. While the GIL model is an improvement over the gas phase approach to calculating the relative anion nucleophilicities proposed here, the gas phase calculations predict the same trend as the GIL method, and could be considered a good first approximation to determining relative anion nucleophilicities.

CONCLUSIONS

The thermal decomposition of alkylimidazolium ionic liquids with CN containing anions has been investigated by multiple, complementary experimental techniques and DFT calculations. Two common thermal decomposition mechanisms have been identified-carbene formation and alkyl abstraction- that are related to anion basicity and nucleophilicity, respectively. A third mechanism, that likely proceeds through the carbene, allows for addition of S or –NCN groups to C2 on the imidazole ring. M06 calculations in the gas phase and the SMD-GIL variant of the polarizable continuum model for the condensed phase have demonstrated the ability to predict trends in anion basicity and anion nucleophilicity which should prove useful in predicting thermal stability trends in dialkylimidazolium ionic liquids and perhaps could be used to predict thermal stabilities of ionic liquids in general.

ACKNOWLEDGEMENTS

We gratefully acknowledge the sample of $EMMIM^{+}dca^{-}$ provided by Stefan Schneider and the GC/MS analysis performed by Amanda Wheaton at the Air Force Research Laboratory. S.D.C. gratefully acknowledges funding from the U.S. Air Force Office of Scientific Research (Grant No. FA9300-06-C-0023).

REFERENCES

(1) Schneider, S., Hawkins, T., Rosander, M., Vaghjiani, G., Chambreau, S. and Drake, G. *Energy and Fuels*, **2008**, *22*, 2871-2872.

(2) Chambreau, S. D., Schneider, S., Rosander, M., Hawkins, T., Gallegos, C. J., Pastewait, M. F. and Vaghjiani, G. L. *Journal of Physical Chemistry A*, **2008**, *112*, 7816-7824.

(3) Kelkar, M. S. and Maginn, E. J. *Journal of Physical Chemistry B*, **2007**, *111*, 9424-9427.

(4) Strasser, D., Goulay, F., Kelkar, M. S., Maginn, E. J. and Leone, S. R. *Journal of Physical Chemistry A*, **2007**, *111*, 3191-3915.

(5) Verevkin, S. P., Zaitsau, D. H., Emel'yanenko, V. N., Yermalayeu, A. V., Schick, C., Liu, H., Maginn, E. J., Bulut, S., Krossing, I. and Kalb, R. *J. Phys Chem. B*, **2013**, *117*, 6473-6486.

(6) Borodin, O., Smith, G. D. and Kim, H. *Journal of Physical Chemistry B*, **2009**, *113*, 4771-4774.

(7) Li, X., Schatz, G. C. and Nesbitt, D. J. *J Phys Chem B*, **2012**, *116*, 3587-3602.
(8) Tomasi, J., Mannucci, B. and Cammi, R. *Chemical Reviews*, **2005**, *105*, 2999-3093.
(9) Maciejewski, J. P., Gao, H. and Shreeve, J. M. *Chem. Eur. J.*, **2013**, *19*, 2947-2950.
(10) Brill, T. B., Brush, P. J., James, K. J., Shepherd, J. E. and Pfeiffer, K. J. *Appl. Spect.*, **1992**, *46*, 900-911.
(11) Thynell, S. T., Gongwer, P. E. and Brill, T. B., **1996**, *12*, 933-939.
(12) Chambreau, S. D., Boatz, J. A., Vaghjiani, G. L., Koh, C., Kostko, O., Golan, A. and Leone, S. R. *Journal of Physical Chemistry A*, **2012**, *116*, 5867-5876.
(13) Chambreau, S. D., Vaghjiani, G. L., Koh, C., Golan, A. and Leone, S. R. *Journal of Puhysical Chemistry Letters*, **2012**, *3*, 2910-2914.
(14) Koh, C., Liu, C.-L., Harmon, C., Strasser, D., Golan, A., Kostko, O., Chambreau, S. D., Vaghjiani, G. L. and Leone, S. R. *Journal of Physical Chemistry A*, **2011**, *115*, 4630-4635.
(15) Zhao, Y. and Truhlar, D. G. *Theor. Chem. Account.*, **2008**, *120*, 215-241.
(16) Izgorodina, E. I., Bernard, U. L. and MacFarlane, D. R. *Journal of Physical Chemistry A*, **2009**, *113*, 7064-7072.
(17) Frisch, M. J., Trucks, G. W., Schlegel, H. B., Scuseria, G. E., Robb, M. A., Cheeseman, J. R., Scalmani, G., Barone, V., Mennucci, B., Petersson, G. A., *et al.* "Gaussian 09, Revision A.02," Gaussian, Inc., 2009.
(18) Marenich, A. V., Cramer, C. J. and Truhlar, D. G. *Journal of Physical Chemistry B*, **2009**, *113*, 6378-6396.
(19) Bernales, V. S., Marenich, A. V., Contreras, R., Cramer, C. J. and Truhlar, D. G. *Journal of Physical Chemistry B*, **2012**, *116*, 9122-9129.
(20) Heym, F., Etzold, B. J. M., Kern, C. and Jess, A. *Physical Chemistry Chemical Physics*, **2010**, *12*, 12089-12110.
(21) Seeberger, A., Andresen, A.-K. and Jess, A. *Physical Chemistry Chemical Physics.*, **2009**, *11*, 9375-9381.
(22) Lou, H., Baker, G. A. and Dai, S. *Journal of Physical Chemistry B*, **2008**, *112*, 10077-10081.
(23) Paulechka, Y. U., Kabo, A. G. and Blokhin, A. V. *J Chem Phys B*, **2009**, *113*, 14742-14746.
(24) Klomfar, J., Souckova, M. and Patek, J. *Journal of Chemical and Engineering Data*, **2012**, *57*, 1213-1221.
(25) Krolikowska, M. and Hofman, T. *Thermochimica Acta*, **2012**, *530*, 1-6.
(26) Carvalho, P. J., Regueira, T., Santos, L. M. B. F., Fernandez, J. and Coutinho, J. A. P. *Journal of Chemical and Engineering Data*, **2010**, *55*, 645-652.
(27) Gardas, R. L., Freire, M. G., Carvalho, P. J., Marrucho, I. M., Fonseca, I. M. A., Ferreira, A. G. M. and Coutinho, J. A. P. *Journal of Chemical and Engineering Data*, **2007**, *52*, 1881-1888.
(28) Wooster, T. J., Johanson, K. M., Fraser, K. J., MacFarlane, D. R. and Scott, J. L. *Green Chemistry*, **2006**, *8*, 691-696.
(29) Chingin, K., Perry, R. H., Chambreau, S. D., Vaghjiani, G. L. and Zare, R. N. *Angew. Chemie Int. Ed.*, **2011**, *50*, 8634–8637.
(30) Lotsch, B. V. and Schnick, W., **2004**, *28*, 1129-1136.

(31) Chambreau, S. D., Vaghjiani, G. L., To, A., Koh, C., Strasser, D., Kostko, O. and Leone, S. R. *Journal of Physical Chemistry B*, **2010**, *114*, 1361-1367.

(32) Johnson, T. J., Sams, R. L. and Sharpe, S. W. "The PNNL quantitative infrared database for gas-phase sensing: a spectral library for environmental, hazmat, and public safety standoff detection"; Proc. SPIE 5269 Chemical and Biological Point Sensors for Homeland Defense, 2004, Providence, RI.

(33) Finnerty, J., Mitschke, U. and Wentrup, C. *Journal Of Organic Chemistry*, **2002**, *67*, 1084-1092.

(34) Köddermann, T., Paschek, D. and Ludwig, R. *ChemPhysChem*, **2008**, *9*, 549-555.

(35) Swiderski, K., McLean, A., Gordon, C. M. and Vaughn, D. H. *Chemical Communications*, **2004**, 2178-2179.

(36) Verevkin, S. P., Emel'yanenko, V. N., Zaitsau, D. H., Heintz, A., Muzny, C. D. and Frenkel, M. *Physical Chemistry Chemical Physics*, **2010**, *12*, 14994-15000.

(37) Zaitsau, D. H., Kabo, G. J., Strechan, A. A., Paulechka, Y. U., Tscherisch, A., Verevkin, S. P. and Heintz, A. *Journal of Physical Chemistry A*, **2006**, *110*, 7303-7306.

(38) Gross, J. H. *Journal of the American Society for Mass Spectrometry*, **2008**, *19*, 1347-1352.

(39) Clough, M. T., Geyer, K., Hunt, P. A., Mertes, J. and Welton, T. *Phys. Chem. Chem. Phys.*, **2013**, *15*, 20480-20495.

(40) Emel'yanenko, V. N., Verevkin, S. P. and Heintz, A. *Journal of the American Chemical Society*, **2007**, *129*, 3930-3937.

(41) Emel'yanenko, V. N., Verevkin, S. P., Heintz, A., Corfield, J.-A., Deyko, A., Lovelock, K. R. J., Licence, P. and Jones, R. G. *Journal of Physical Chemistry B*, **2008**, *112*, 11734-11742.

(42) Emel'yanenko, V. N., Zaitsau, D. H., Verevkin, S. P., Heintz, A., Vos, K. and Schultz, A. *Journal of Physical Chemistry B*, **2011**, *115*, 11712-11717.

(43) Fumino, K., Wulf, A., Verevkin, S. P., Heintz, A. and Ludwig, R. *ChemPhysChem*, **2010**, *11*, 1623-1626.

(44) Armstrong, J. P., Hurst, C., Jones, R. G., Licence, P., Lovelock, K. R. J., Satterly, C. J. and Villar-Garcia, I. J. *Phys. Chem. Chem. Phys.*, **2007**, *9*, 982-990.

(45) Holloczki, O., Gerhard, D., Massone, K., Szarvas, L., Nemeth, B., Veszpremi, T. and Nyulaszi, L. *New J. Chem.*, **2010**, *34*, 3004-3009.

(46) Rodriguez, H., Gurau, G., Holbrey, J. D. and Rogers, R. *Chemical Communications*, **2011**, *47*, 3222-3224.

(47) Koppel, I. A., Taft, R. W., Anvia, F., Hu, L.-Q., Sung, K.-S., DesMarteau, D. D., Yagupolskii, L. M., Yagupolskii, Y. L., Ignat'ev, N. V., Kondratenko, N. V., *et al. Journal of the American Chemical Society*, **1994**, *116*, 3047-3057.

(48) Arduengo, A. J., Harlow, R. L. and Kline, M. *Journal of the American Chemical Society*, **1991**, *113*, 361-363.

(49) Igau, A., Grutzmacher, H., Baceiredo, A. and Bertrand, G. *Journal of the American Chemical Society*, **1988**, *110*, 6463-6466.

(50) Wanzlick, H. W. and Schonherr, H. J. *Liebigs Annalen der Chemie*, **1970**, *731*, 176-179.

(51) Lias, S. G. Ionization Energy Evaluation. In *NIST Chemistry WebBook, NIST Standard Reference Database Number 69*; Linstrom, P. J., Mallard, W. G., Eds.; National Institute of Standards and Technology.

(52) Chowdhury, A. and Thynell, S. T. *Thermochimica Acta*, **2006**, *443*, 159-172.

(53) Kan, H.-C., Tseng, M.-C. and Chu, Y.-H. *Tetrahedron*, **2007**, *63*, 1644-1653.

(54) Stein, S. E. Infrared Spectra Gaithersburg, MD, 2014.

(55) Kroon, M. C., Buijs, W., Peters, C. J. and Witkamp, G.-J. *Thermochimica Acta*, **2007**, *465*, 40-47.

(56) Edwards, J. O. *Journal of the American Chemical Society*, **1953**, *76*, 1540-1547.

Supplemental Information

BMIM$^+$dca$^-$

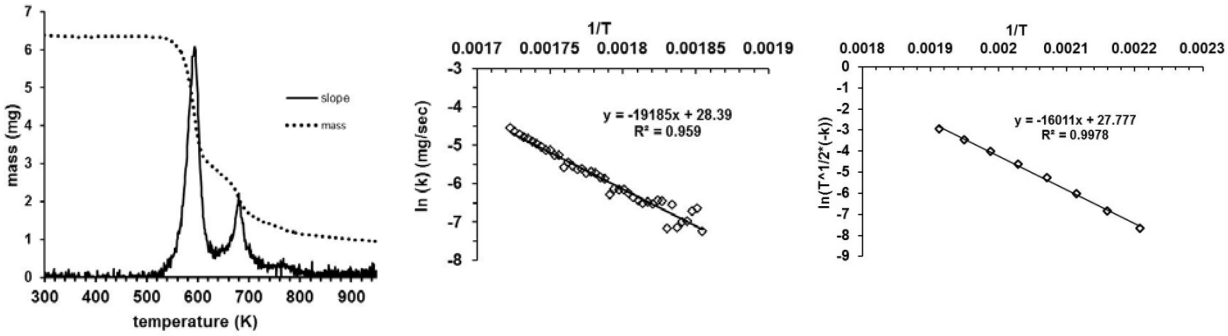

Figure S1. TGA measurements for BMIM$^+$dca$^-$: a) non-isothermal TGA, b) ΔH(overall) from (a), c) ΔH_{vap} from isothermal TGA.

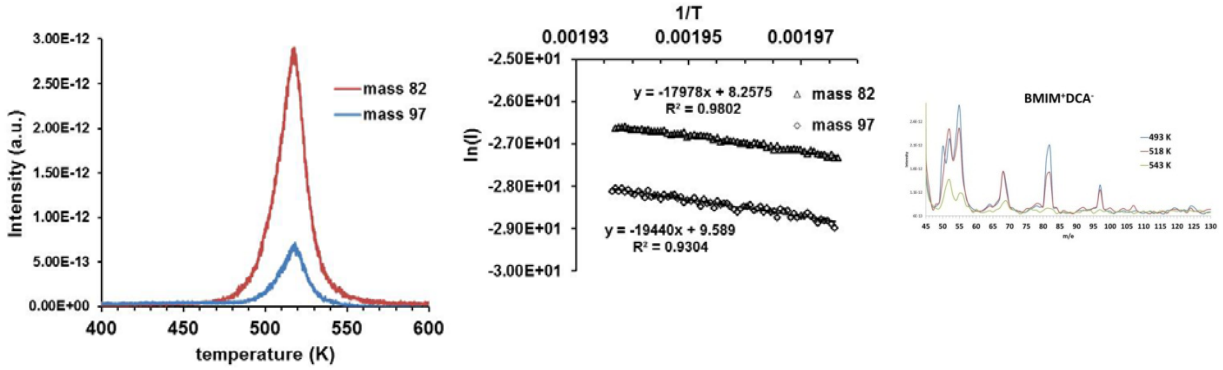

Figure S2. a) TGA-MS of m/z 97 and 82, and b) $\Delta H^{\ddagger}$ of product formation, and c) complete TGA-MS at 493, 518 and 543 K.

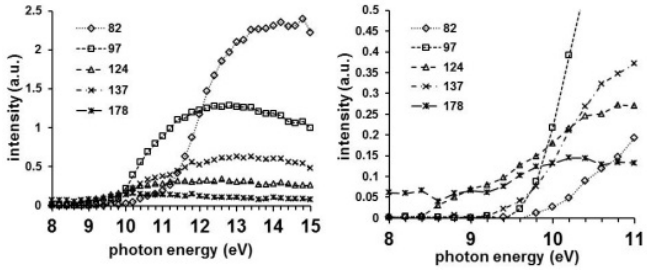

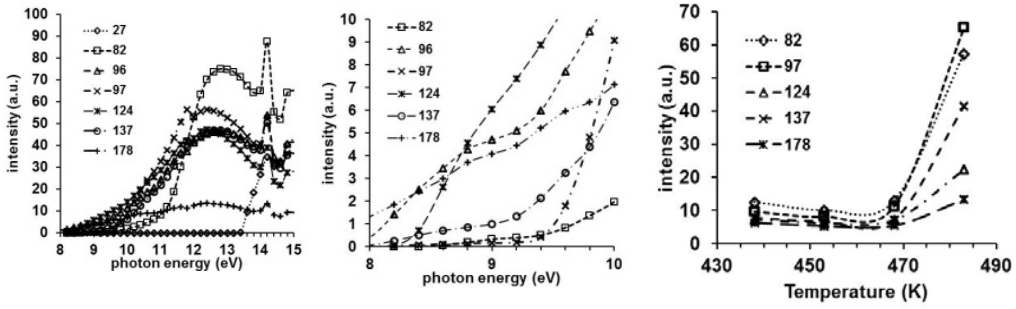

Figure S3. VUV-PI-TOFMS of $BMIM^+dca^-$ a) at 438 K, b) an expanded view of (a), c) at 483 K, d) an expanded view of (c), and e) temperature profiles of photoion peak intensities.

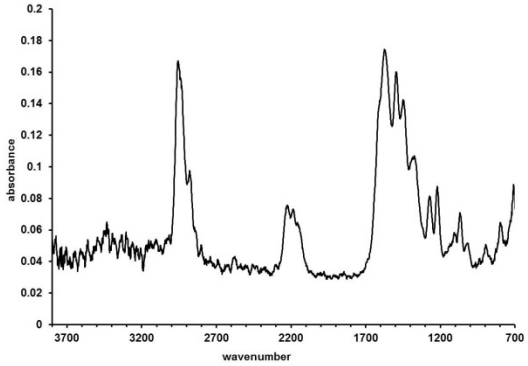

Figure S4. T-jump experiment of $BMIM^+dca^-$.

$EMMIM^+dca^-$

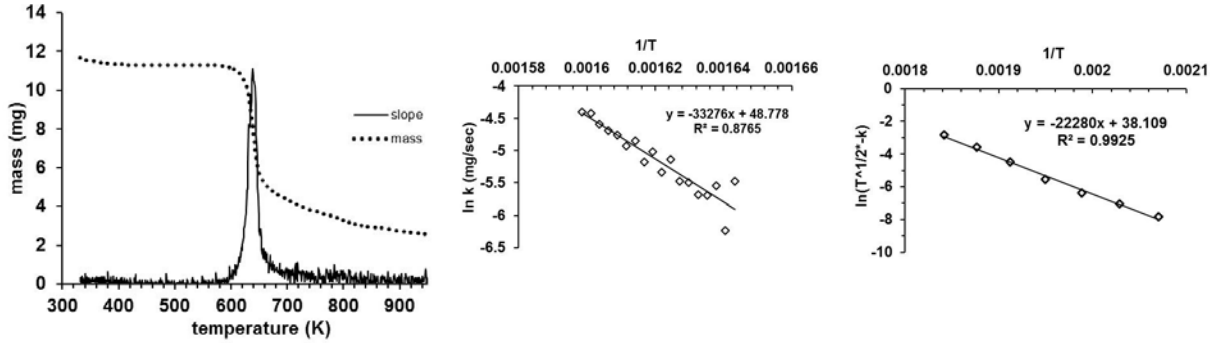

Figure S5. TGA measurements for $EMIM^+dca^-$: a) non-isothermal TGA, b) ΔH(overall) from (a), c) ΔH_{vap} from isothermal TGA.

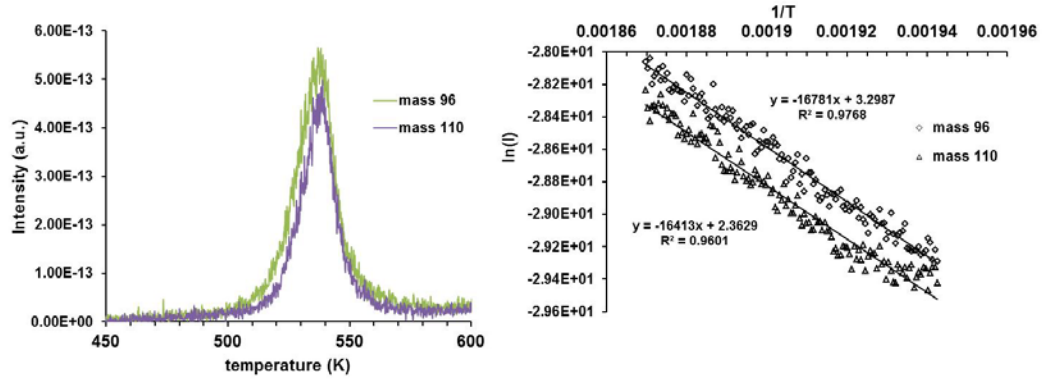

Figure S6. a) TGA-MS of m/z 96 and 110, and b) $\Delta H^{\ddagger}$ of product formation in (a).

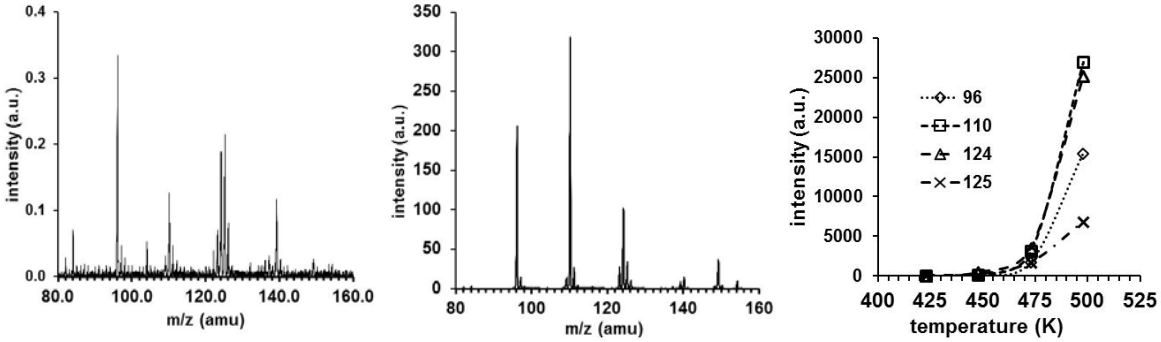

Figure S7. VUV-PI-TOFMS of $EMMIM^{+}dca^{-}$ a) at 423 Kand 10.0 eV, b) at 498 K and 10.0 eV, and c) temperature profiles of photoion peak intensities.

$EMIM^{+}SCN^{-}$

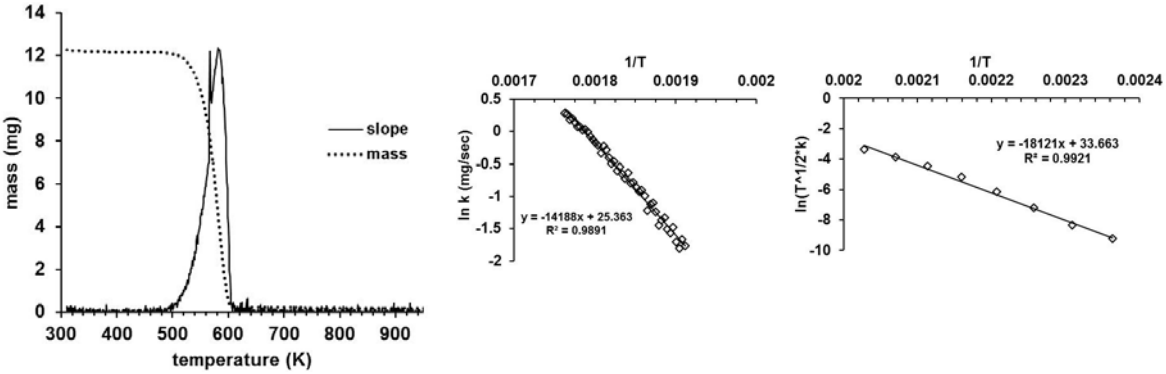

Figure S8. TGA measurements for $EMIM^{+}SCN^{-}$: a) non-isothermal TGA, b) ΔH(overall) from (a), c) ΔH_{vap} from isothermal TGA.

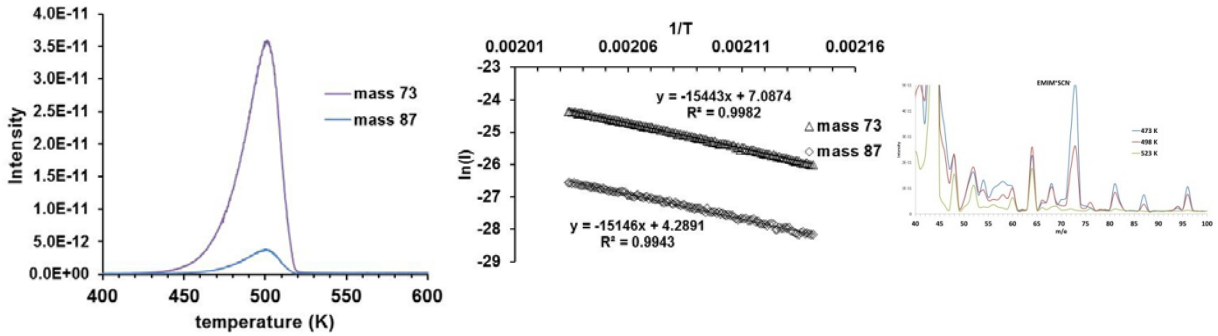

Figure S9. a) TGA-MS of m/z 73 and 87, b) $\Delta H^{\ddagger}$ of product formation in (a), and c) complete TGA-MS at 473, 498 and 523 K.

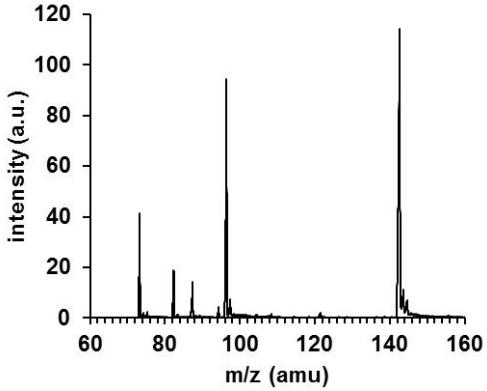

Figure S10. VUV-PI-TOFMS of $EMIM^{+}SCN^{-}$ at 467 K and 10.0 eV.

$BMIM^{+}SCN^{-}$

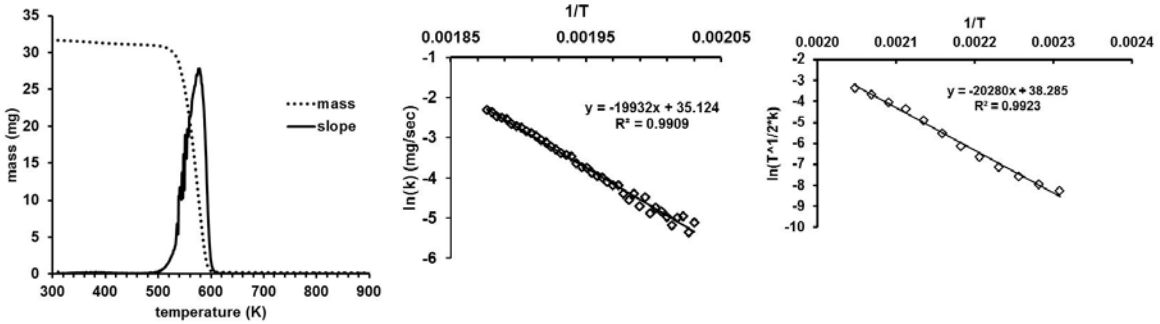

Figure S11. TGA measurements for $BMIM^{+}SCN^{-}$: a) non-isothermal TGA, b) ΔH(overall) from (a), c) ΔH_{vap} from isothermal TGA and d) TGA-MS.

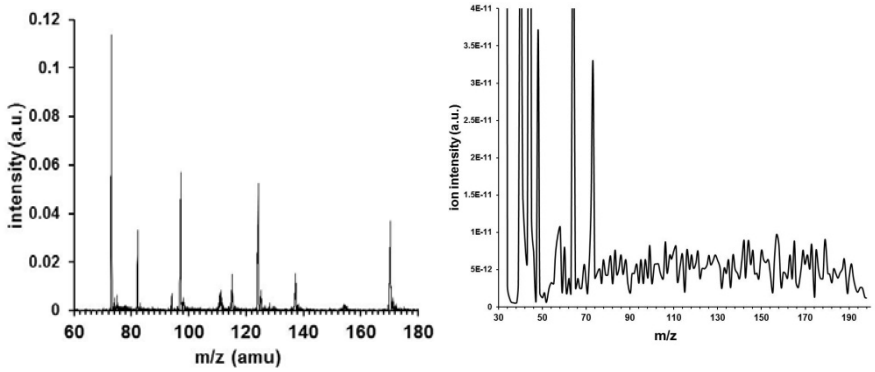

Figure S12. VUV-PI-TOFMS of $BMIM^{+}SCN^{-}$ at 499 K and 10.0 eV.

BMIM$^+$TCM$^-$

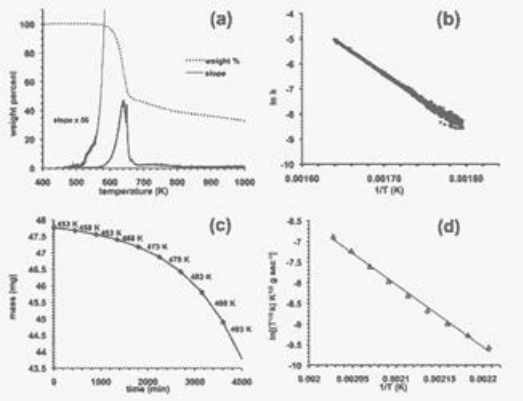

Figure S13. TGA measurements for BMIM$^+$TCM$^-$: a) non-isothermal TGA, b) ΔH(overall) from (a), c) isothermal TGA, and d) ΔH_{vap} from isothermal TGA. (reproduced from J Phys Chem Lett, used with permission).

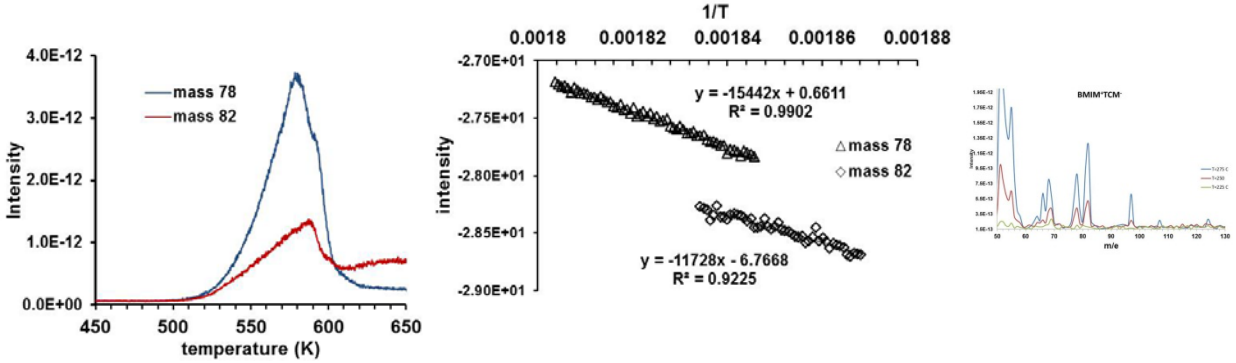

Figure S14. a) TGA-MS of m/z 78 and 82, b) $\Delta H^{\ddagger}$ of product formation in (a), and c) complete TGA-MS at 498, 523 and 548 K.

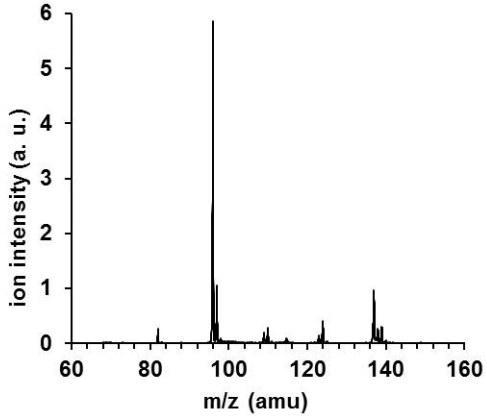

Figure S15. VUV-PI-TOFMS of BMIM$^+$TCM$^-$ at 433 K and 10.0 eV.

BMIM$^+$vdca$^-$

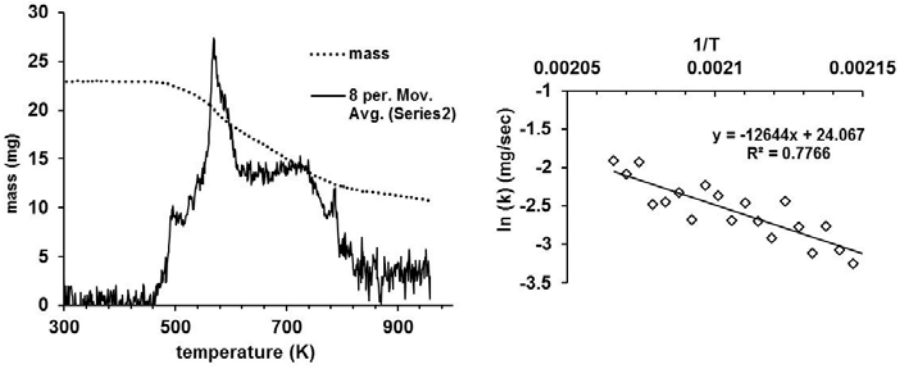

Figure S16. TGA measurements for BMIM$^+$vdca$^-$: a) non-isothermal TGA, b) Δ*H*(overall) from (a).

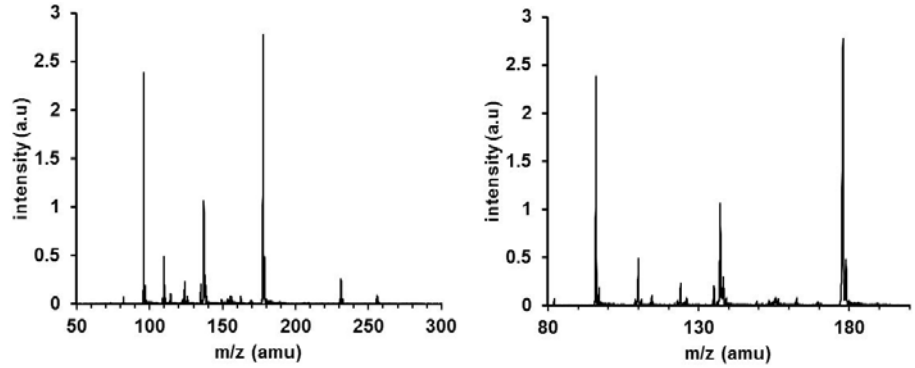

Figure S17. VUV-PI-TOFMS of BMIM$^+$vdca$^-$ at 413 K and 9.0 eV.

BMMIM$^+$dca$^-$

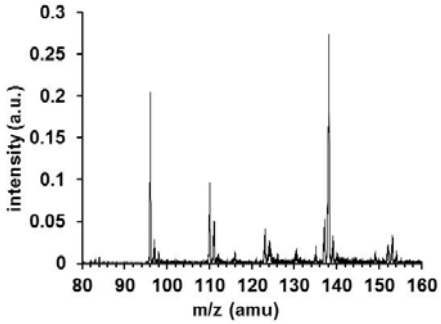

Figure S18. VUV-PI-TOFMS of BMIM$^+$vdca$^-$ at 523 K and 10.0 eV.